Graphite electrode-based CO_2-thermal plasma gasification of plastic waste towards hydrogen-rich syngas production: A techno-environmental perspective

Tejashwi Rana[1], Aishik Basu Mallick[1], Kaushik Kundu[2], Kamal K. Pant[2,3], Satyananda Kar[1*]

[1] Department of Energy Science and Engineering, Indian Institute of Technology Delhi, Hauz Khas, New Delhi, 110016, India

[2] Department of Chemical Engineering, Indian Institute of Technology Delhi, Hauz Khas, New Delhi, 110016, India

[3] Department of Chemical Engineering, Indian Institute of Technology Roorkee, Uttarakhand – 247667, India

*satyananda@dese.iitd.ac.in

Abstract

Plastic waste mitigation and advancing the hydrogen economy are urgent global priorities. Plasma gasification evolves as an advanced process in waste-to-energy technology. However, existing thermal plasma gasification studies frequently rely on oversimplified thermodynamic models that treat the plasma arc merely as a generic heat source. Bridging this critical research gap a novel model was developed in ASPEN PLUS v14.0. This study introduces a synergistic, carbon-negative pathway for low-density polyethylene valorization using a graphite electrode-based Ar-CO_2 thermal plasma. The model was validated against an in-house lab-scale reactor to evaluate the performance of different gasification agents, including CO_2, steam, and their mixtures. Thermodynamic analysis identified a mixed gasification agent (0.75 kg/h steam and 0.25 kg/h CO_2) as the optimal configuration. Under these conditions, high carbon conversion was achieved with syngas purity reaching 95.6 vol%, consisting mainly of 52.0 vol% H_2 and 43.6 vol% CO, while CO_2 formation was limited to 1.18 vol%. The process produced 4.30 Nm^3/kg of syngas with a cold gas efficiency of 74.8%. Energy analysis showed a specific energy consumption of 4.04 kWh/Nm^3 of H_2 at the laboratory scale, which decreases to 1.35 kWh/Nm^3 of H_2 when scaled to a 10 kg/h pilot system. Integration of carbon capture and utilization using pressure swing adsorption enabled CO_2 recovery and recirculation, resulting in a net emission of only 0.06 kg CO_2/kg plastic. This represents an 88% reduction compared with conventional incineration. The proposed mixed-agent plasma gasification pathway therefore offers a promising low-carbon route for hydrogen-rich syngas production from plastic waste.

Keywords: LDPE; Plasma gasification, Thermal plasma, ASPEN PLUS simulation, Hydrogen economy, CCU.

1. Introduction

Plastic waste has become one of the most pressing environmental challenges of the twenty-first century [1]. Global production of plastics exceeded 400 million tonnes (Mt) in 2022, double the production of 2002. Recent studies predict a 2 to 3 fold increase by 2050, resulting in an inevitable rise in volume from 902 Mt [2] to 1124 Mt [3]. The continuous annual growth results in vast amounts of post-consumer and industrial plastic waste entering landfills, oceans, and natural environments [4,5]. Conventional waste management systems struggle to cope with the heterogeneity and persistence of plastic polymers, leading to severe ecological impacts and long-term pollution problems [6]. Despite recycling efforts, only a small fraction of plastic waste is successfully reused, while the majority are incinerated or landfilled [7]. This trajectory has profound implications for soil contamination, marine pollution, microplastic proliferation, and greenhouse gas emissions, emphasizing the urgent need for sustainable and scalable plastic waste valorization methods [8].

Plasma gasification has emerged as an advanced thermochemical technology capable of overcoming the limitations of conventional technologies [9]. It employs an electrical discharge, typically through a thermal arc, to generate a high-energy ionized gas known as plasma. The unique properties of plasma, characterized by extremely high temperatures (often exceeding 10,000 °C) and a mixture of highly reactive species, including electrons, ions, and radicals, facilitate rapid and complete decomposition of complex organic molecules [10]. The high enthalpy and reactive species in thermal plasma environments enhance reaction kinetics and significantly suppress the formation of undesirable byproducts such as tar and soot [11]. Plasma gasification also produces vitrified inert slag from inorganic components, reducing hazardous residues [12]. Fundamentally, plasma can be generated by various energy sources such as alternating current (AC) [13], direct current (DC) [14], radiofrequency (RF) [15], and microwave systems [16,17]. Among these, DC arc plasma torches are widely used in waste gasification due to their simplicity, effective arc stabilization, and capability to generate extremely high temperatures [18].

A critical parameter in plasma gasification is the choice of plasma-forming gas, which affects the plasma's thermodynamic and chemical behavior. Common gases used for plasma generation include air, nitrogen (N_2), argon (Ar), steam, and carbon dioxide (CO_2) [19]. Air and nitrogen are economical, but nitrogen dilution lowers syngas calorific value and introduces nitrogen oxides (NO_x) emissions [20]. Argon provides inert plasma conditions with high temperatures, yet its cost is prohibitive for large-scale applications. Steam enhances hydrogen

production through steam reforming reactions but demands additional energy requirements in the process. In recent years, CO_2 has gained attention as a plasma-forming gas due to its dual role as both a heat carrier and a reactive species (gasification agent) [21]. Experimental studies have demonstrated that CO_2 plasma gasification can achieve higher hydrogen yields (42−79 vol%), depending on operating conditions and feedstock composition [22]. Comparative studies between CO_2 and other carrier gases have revealed several key advantages of CO_2 plasma gasification [21]. CO_2 plasma operates in a controlled atmosphere that promotes gasification rather than combustion, eliminating nitrogen dilution, and significantly reducing nitrogen oxide formation [23]. The decomposition of CO_2 contributes to additional CO formation, which improves the calorific value of syngas [24]. Furthermore, utilizing CO_2 as a gasifying medium supports greenhouse gas mitigation strategies by capturing and converting it into valuable energy carriers within the gasifier.

The choice and design of electrode materials in plasma torches represent another critical aspect of system performance [19]. Conventional metallic electrodes such as copper, tungsten, and their alloys are widely used for plasma generation due to their high electrical conductivity and robustness. Tungsten, in particular, is a common electrode material because of its high melting point and arc stability [25]. However, metallic electrodes require substantial cooling, often through water jackets, to prevent melting and prolong electrode life. For instance, Ruj et al. observed that more than half of the electrical energy in a thermal plasma system is removed by cooling water [26]. Sikarwar et al. measured the electrical efficiencies of the plasma torch at 67−69 %, corresponding to 31−33 % cooling losses [27]. Similarly, Aikas et al. quantified the energy balance in a DC plasma torch and found that about 52% of input energy was transferred to the anode and cathode cooling water streams [28]. These consistent findings support the statement that 30−55 % of total input energy is typically lost to cooling systems in high-temperature plasma torches.

To mitigate such energy losses, non-metallic electrodes like graphite have been explored as alternatives [19]. Graphite offers excellent high-temperature stability and thermal conductivity, reducing the need for intense cooling systems [29]. Without water-cooling, graphite electrodes can sustain operation in extreme thermal environments, potentially improving the energy efficiency of plasma gasification systems. Graphite electrodes also distribute heat more evenly, reducing thermal stress and extending electrode lifespan [30]. Nevertheless, graphite erosion under high-temperature oxidative conditions and complex arc dynamics represents challenges that require further investigation.

In the context of plastic waste processing, plasma gasification stands out as a promising solution that addresses key limitations of conventional processes [31]. It offers high conversion efficiency [21], minimal tar production [32], and the potential for clean energy recovery [27]. However, substantial gaps remain in understanding the interaction between CO_2 thermal plasma and graphite electrodes. To evaluate and optimize these advanced thermochemical systems, researchers rely on process simulators like ASPEN PLUS. However, a critical limitation pervades the existing literature regarding the simulation of plasma gasification: the oversimplification of the plasma torch [33,34]. Most current models treat the plasma arc merely as a generic, idealized heat source [35]. This abstraction ignores the fundamental physics of plasma generation, failing to account for thermal dissociation of the carrier gas, the energetic losses of electron quenching and recombination, and the endothermic sublimation of the electrodes [24]. Overlooking the plasma core's function as an intense chemical pre-processor causes reported models to inaccurately depict the physical reactor's real-world thermodynamic constraints, kinetic barriers, and energy demands. Another software used for DC thermal arc plasma generation is COMSOL [36,37]. However, the simulation study of interaction of plasma with waste is very limited using other software.

To bridge these substantial gaps, this study presents a comprehensive experimental and theoretical investigation of thermal plasma gasification of low-density polyethylene (LDPE). A novel ASPEN PLUS thermodynamic model was developed to exclusively mimic the actual thermal arc plasma gasification process. By explicitly simulating carrier gas dissociation, discrete thermal gradient zones, and electrode sublimation, the model provides a highly rigorous framework for predicting syngas quality. This study systematically evaluates three distinct gasification scenarios: CO_2 gasification (Model I, validated through in-house physical experiments), steam gasification (Model II, validated with reported experimental data), and a highly synergistic mixed gasification agent approach utilizing both steam and CO_2 (Model III). To demonstrate the reliability of the technology, a holistic techno-environmental assessment is conducted. This encompasses operational performance metrics (specific syngas yield, cold gas efficiency, lower heating value, carbon conversion efficiency, etc.), environmental carbon footprint benchmarking, and integration of carbon capture and utilization (CCU) model for net-zero carbon processing. Finally, a preliminary study including hydrogen yield and specific energy consumption (SEC) projections was performed to demonstrate the industrial viability of the technology towards the upcoming hydrogen economy.

2. Materials and methods

This section outlines the comprehensive experimental and theoretical methodologies employed to investigate the DC thermal arc plasma gasification of LDPE waste. It details the laboratory-scale physical reactor setup, encompassing the electrode configuration, carrier gas supply system, and the diagnostic techniques utilized to characterize plasma plume dynamics, preheating stability, and real-time syngas composition. Building upon this empirical foundation, the section subsequently elaborates on the development of a novel ASPEN PLUS thermodynamic simulation.

2.1 The experimental setup

A laboratory-scale plasma gasification system with a processing capacity of 5 kg/h was designed and developed to convert plastic waste into clean energy products as shown in Figure 1. The core of the system is a plasma gasification chamber, configured similarly to a fixed-bed updraft reactor. The chamber has an inner diameter of 150 mm and a height of 1000 mm, internally lined with 150 mm of high-alumina refractory bricks capable of withstanding temperatures up to 1700 °C. The outer shell was constructed from 5 mm-thick mild steel for structural integrity. The experimental setup comprises several integrated components, including the plasma chamber, DC power supply (450A, 75V), thermocouple ports, gas inlet and outlet ducts, screw conveyor, condenser, cyclone separator, venturi scrubber, biomass filter, and a gas storage compressor. The graphite electrodes are positioned horizontally and face each other, with cathodes of 36 mm and an anode of 65 mm diameter. Various carrier gases such as argon (Ar), carbon dioxide (CO_2), and Ar-CO_2 mixtures are introduced through a 10 mm diameter gas inlet port located 100 mm below the electrode gap and oriented perpendicular to the electrode alignment. Additionally, nitrogen (N_2) is employed as a purge gas to minimize oxidation and prevent combustion within the plasma zone. A thermal arc plasma is generated between the electrodes by the DC power supply, creating a high-temperature environment for effective decomposition of plastic waste. The evolved gases are directed to a condenser for cooling and subsequently drawn under negative pressure into a gas purification train comprising a cyclone separator, a venturi scrubber, and a biomass filter to remove particulates, fly ash, and other impurities. The purified syngas is finally stored at 12 bars in a 20-liter compressor-based storage unit for subsequent compositional and performance analyses. A schematic diagram of the plasma gasification system is presented in Figure 1.

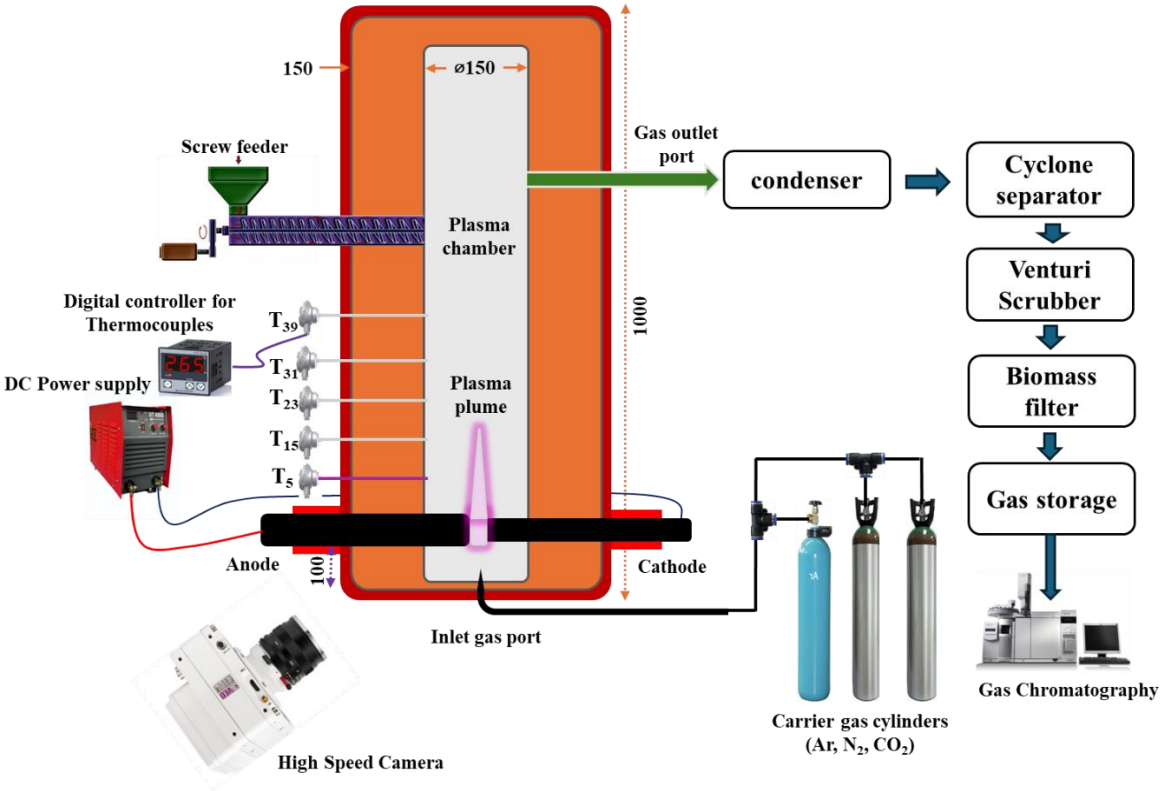

Figure 1. Schematic diagram of an Ar-CO_2 thermal plasma gasification setup for plastic waste processing (all dimensions are in mm).

2.2 Methodology

This section outlines the characterization of feedstock, comprehensive diagnostic, analytical, and theoretical frameworks utilized to evaluate the thermal arc plasma gasification system. It demonstrates measurement techniques for key operating parameters, including thermal profiling, electrical energy input, carrier gas flow rates, and high-speed imaging of plasma plume dynamics. The methodology encompasses the protocols for the plasma chamber preheating study, along with rigorous characterization of the product syngas.

2.2.1 Feedstock characterization

Low-density polyethylene (LDPE) plastic waste, commonly used in grocery carry bags and packaging films, was selected as the feedstock for this study. The LDPE plastic waste (polybags) was collected from community waste bins and manually segregated to remove foreign materials. The collected material was thoroughly washed with water to remove dirt and adhering contaminants and subsequently sun-dried to eliminate surface moisture. The dried plastic was then shredded into smaller pieces to ensure uniform feeding and representative sampling. Representative samples were prepared using standard sampling procedures and

subjected to proximate and ultimate analyses to determine their physicochemical characteristics.

2.2.2 Operating parameters measurement

B-type and K-type thermocouples, with maximum operating limits of 1800 °C and 1200 °C, respectively, were employed to monitor the plasma chamber wall temperature. Five thermocouple ports were positioned axially above the electrode plane at 5, 15, 23, 31, and 39 cm, denoted as T_5, T_{15}, T_{23}, T_{31}, and T_{39}, respectively and 5 mm inside the reactor from the internal diameter. The B-type thermocouple was installed at T_5, closest to the plasma zone, to withstand the highest thermal load. The thermocouples were calibrated using a Bosch GHG180 heat gun as the heat source, with a FLIR E63900 thermal camera. The calibration showed deviations of ±3 °C for the K-type and ±5 °C for the B-type thermocouples, and these corrections were applied to all experimental temperature measurements. The thermocouple placements were sufficiently distant from the plasma region, eliminating the need for additional thermal shielding or insulation.

The total energy input (kWh) was determined by integrating the product of average voltage (V_{avg}) and current (I_{avg}) over the preheating time (t) required to reach 850 °C, expressed in Equation 1 as:

$$E = \int V \cdot I \, dt \approx V_{avg} \times I_{avg} \times t \qquad (1)$$

During the experiment, the current was maintained at 300 A, while the voltage varied with changes in the electrode gap caused by gradual electrode erosion. The voltage fluctuation of ±2 V under steady conditions resulted in an estimated uncertainty of ±5 % in the energy input calculation.

The flow rates of carrier gases (Ar, CO_2) and the purge gas (N_2) were measured using calibrated flow meters compatible with each gas type to ensure precision and reliability. Calibration was performed with Alicat Scientific mass flow controllers (Model: MCR-50SLPM-D-DB9M/5M), incorporating temperature and pressure compensation for STP-standardized readings. CO_2 expansion at atmospheric pressure caused cooling and condensation in the delivery line; a heating unit was employed to preheat the gas to ambient temperature, ensuring stable gas-phase injection comparable to that of Ar and N_2.

2.2.3 High-speed imaging characterization of plasma plume

The plasma plume characteristics were analyzed using sequential images captured by a high-speed Phantom VEO410L camera (12-bit, 1 MP sensor) fitted with an F-Mount Nikkor

Macro Lens (24−85 mm, f/2.4−4). The camera recorded the plume motion at 5000 fps with a 520 × 480 resolution and an exposure interval of 150 μs, producing approximately 8000 frames corresponding to 1.3 seconds of real-time footage. The camera was positioned ~300 mm from the plasma zone and remained stationary during the entire observation. Image frames were extracted and analyzed using Cine Viewer v3.7 and ImageJ software. Spatial calibration was achieved using the known diameter of the graphite electrode, establishing a scale of 48 pixels/cm.

2.2.4 Preheating temperature study

The plasma chamber was preheated using CO_2, Ar, and Ar-CO_2 gas mixtures as carrier gases to achieve a target temperature of 850 °C prior to waste feeding. This temperature was chosen to inhibit the formation of toxic byproducts such as polychlorinated dibenzodioxins (PCDDs) and polychlorinated dibenzofurans (PCDFs), which predominantly form in the 200−800 °C range, with maximum formation near 350−400 °C. Since their generation becomes thermodynamically negligible above 800 °C, maintaining 850 °C provided a 50 °C safety margin, ensuring environmentally safe preheating before introducing waste. Nitrogen gas was used as a purge medium in all experiments to suppress oxidation reactions that could accelerate electrode erosion and promote unwanted CO_2 formation. A 30 LPM nitrogen flow for 10 minutes was sufficient to establish a reduced-oxygen environment before arc initiation. The plasma arc was ignited by spark formation at a current of 50 A, electrode gap of 0.1 cm, and voltage of 10±1 V. The voltage required for transition from spark to stable plasma (gap of 0.5 cm) was lower for argon (15±2 V) than for CO_2 (25±3 V) due to argon's lower ionization energy, while Ar-CO_2 mixtures required intermediate voltages (20±2 V). Experimental observations indicated that currents below 250 A were insufficient for effective chamber preheating. In argon discharges, the plasma plume only extended 1−2 cm beyond the electrode tip, providing inadequate heating, whereas in CO_2 discharges, the arc remained localized between electrodes. Stable plasma formation was achieved from 250−300 A for argon, but pure CO_2 plasma remained thermally unstable.

To improve stability of plasma, Ar is mixed with CO_2 in several proportions and achieved stability condition at Ar flow rate of 10 LPM and CO_2 of 5 LPM. The formation of Ar-CO_2 thermal arc plasma relies on establishing a stable, high-temperature discharge at atmospheric pressure, where argon's inert and conductive nature facilitates plasma initiation. Argon's lower ionization potential enhances electrical conductivity, enabling efficient energy transfer and sustaining high-temperature reactions. Through Penning ionization and charge exchange,

metastable Ar atoms (Ar*) energize CO_2 molecules, promoting dissociation and stabilizing the plasma at lower voltages than required for pure CO_2. At the same time, pure CO_2 plasmas exhibit instability due to high ionization energy, rapid cooling, and energy losses via vibrational and rotational excitations. The addition of argon mitigates these effects by improving thermal conduction, reducing arc extinction, and enabling uniform plasma formation, thus supporting efficient gas-phase conversion and stable high-temperature operation [24].

2.2.5 Characterisation of gas

A gas collection system, incorporating a compressor positioned downstream of the cooling and cleaning units (Figure 1), was used to maintain negative pressure in the plasma chamber and ensure a steady gas flow. Periodic gas samples were collected using a tedlar bag (0.5 L) to minimize uncertainty, and gas composition analysis was performed using Thermo Scientific (Model: Trace 1110) gas chromatograph (GC). Prior to the experimental runs, the GC was rigorously calibrated using certified multi-component standard gas mixtures to establish baseline reference peaks, ensuring high quantitative accuracy and reliable peak integration for the product syngas. Two sampling methods, direct sampling and indirect (from compressor) sampling, were compared to verify data reliability. In a direct sampling condition, gases were directly drawn from the reactor through a gas collection probe connected to diaphragm compressor, cooled in a copper helical coil, collected in a tedlar bag and analyzed using gas analyzer (GC). Whereas, in an indirect method, gases were collected from a compressor (storage facility of 20 L) tank maintained near atmospheric pressure (output valve of compressor was kept open) to ensure continuous renewal. Both techniques yielded consistent results within ± 2 % across major species (H_2, CO, CH_4, CO_2), confirming the absence of oxidation or adsorption effects during gas sampling.

Specific syngas yield (SSY) is a vital industrial metric that defines the physical quantity of the combustible product gas generated per unit mass of feedstock processed. It is calculated by dividing the total volumetric flow rate of the dry product syngas by the mass feed rate. It is expressed in standard cubic meters per kilogram (Nm^3/kg) using the following Equation 2:

$$SSY\ (Nm^3/kg) = \frac{V_{Syngas}}{m_{feed}} \qquad (2)$$

Where V_{syngas} is the total volume flow rate of dry syngas (Nm^3/h) (excluding condensed water vapor) and m_{feed} is the constant mass feed rate of the plastic waste (1.0 kg/h).

The lower heating value (LHV) of produced gas, cold gas efficiency (CGE), and carbon conversion efficiency (CCE) are used as parameters to assess the quality of output and operation performance. The LHV of gas is calculated based on the composition of the produced gas. It is the total heat released during the complete combustion of a fuel, computed using Equation 3 [38].

$$LHV_{\ product\ gas} = 10.79\, Y_{H_2} + 12.63\, Y_{CO} + 35.83\, Y_{CH_4} \qquad (3)$$

Where Y_{H_2}, Y_{CO}, Y_{CH_4}, are the percentage of gas in the composition of product gas and $LHV_{\ product\ gas}$ is the lower heating value of product gas (MJ/Nm^3).

Cold gas efficiency (CGE) is used to determine the energy efficiency of the waste treatment process as expressed in Equation 4 [39].

$$CGE = \frac{\dot{m}_{product\ gas} \times LHV_{product\ gas}}{(\dot{m}_{feed} \times LHV_{feed}) + P_{in}} \qquad (4)$$

where $\dot{m}_{product\ gas}$is the mass flow rate of product gas (m^3/kg), $LHV_{\ product\ gas}$ is the lower heating value of product gas (MJ/Nm^3), $\dot{m}_{feed}$ is the mass flow rate of feed, LHV_{feed} is the lower heating value of feed (MJ/kg), and P_{in} is the plasma power input (kW).

Carbon conversion efficiency (CCE) is used to determine the chemical efficiency of the waste treatment process. It is a fundamental performance metric that quantifies the fraction of solid carbon present in the raw feedstock that is successfully volatilized and transformed into permanent product gases (such as CO, CO_2, and CH_4). The CCE is calculated using the following Equation 5 [40,41].

$$CCE = \frac{(V_{syngas}\ x\ (Y_{CO} + Y_{CO_2} + Y_{CH_4})\ x \frac{12}{22.4})}{(m_{feed}\ x\ Y_C)} \qquad (5)$$

Where Y represents the volume fractions of the respective carbonaceous gases. $\frac{12}{22.4}$ is the molar mass of carbon (~12 kg/kmol) per standard molar volume (22.4 Nm^3/kmol). Y_c is the mass fraction of carbon inherent to the LDPE feedstock (0.734, as established in Table 1).

Hydrogen yield measures the absolute volume of H_2 gas produced per kilogram of processed plastic waste. It is derived by multiplying the total SSY by the hydrogen volume fraction in the dry syngas, as shown in Equation 6 [42].

$$H_2\ yield\ (Nm^3/kg) = \frac{V_{syngas} \times Y_{H_2}}{m_{feed}} \qquad (6)$$

The specific energy consumption (SEC) of H_2 production evaluates the energy efficiency of the H_2 generation process. It quantifies the amount of plasma electrical energy required to produce one normal cubic meter of H_2 gas, providing a direct metric for commercial scale-up and economic feasibility. The SEC was computed using Equation 7, where E_{in} is the electrical energy input from the DC power supply [42].

$$SEC\ (kWh/Nm^3\ H_2) = \frac{E_{in}}{V_{syngas} \times Y_{H_2}} \quad (7)$$

2.2.6 Optical emission spectroscopy characterisation

Optical emission spectroscopy (OES) was used to monitor molecular and atomic transitions using an Ocean Optics HR4 Pro spectrometer (0.9 nm resolution, 10 μm slit, 200−1100 nm range). A 200 μm optical fiber, positioned 30 cm from the plasma core, collected emissions under steady alignment for all conditions. Spectra were recorded at a 15 μs integration time, with scan averaging triplicate and boxcar smoothing (width = 5). Background corrections were applied before acquisition, and emission peaks corresponding to Ar, CO_2, CO, and O were identified by matching observed wavelengths to NIST spectral data, supporting the results of the gas composition analysis.

2.3 ASPEN PLUS model development

The simulation of the plasma gasification process was developed using ASPEN PLUS process simulation software. The model evaluates the thermodynamic limits and syngas composition resulting from the high-temperature conversion of LDPE. Due to the presence of high-temperature gas-phase species and the non-ideal behavior of the mixture under plasma conditions, the Peng-Robinson equation of state with Boston-Mathias alpha function (PR-BM) was selected as the global thermodynamic property method. The LDPE feedstock, being a non-standard material, was defined as a non-conventional component. Its thermodynamic properties were calculated based on ultimate and proximate analyses using the HCOALGEN and DCOALIGT property models in ASPEN PLUS.

2.3.1 Ar-CO_2 thermal arc plasma generation modelling

A critical limitation in many reported simulation studies on plasma gasification is the oversimplification of the plasma torch, which is frequently modelled as a generic, ideal heat source. To bridge this gap and accurately reflect the experimental setup, this study introduces a detailed thermodynamic model of the thermal arc plasma generation process. An Ar-CO_2 mixture is utilized as the plasma-forming gas. The mass flow rates for both streams are directly

extracted from the experimental baseline data. In the physical experiments, the extreme temperatures and high-energy electron collision the arc core does not simply heat the CO_2; they fundamentally alter its chemical structure. Considering this aspect, the plasma generation is modeled in ASPEN PLUS using an initial, ultra-high-temperature RGibbs reactor (designated as TORCH in Figure 2). By defining the core temperature at extreme levels (exceeding 8000 K), this block acts as a chemical pre-processor rather than just a heater. Under these conditions, the model calculates the thermodynamic equilibrium of the carrier gas dissociation, capturing the essential physics of the thermal plasma:

- Carrier gas dissociation: The molecular CO_2 is subjected to thermal and electron-impact dissociation. The model accurately predicts the breakdown of CO_2 into a highly reactive mixture of carbon monoxide (CO), molecular oxygen (O_2), highly reactive monoatomic oxygen radicals (O), and residual undissociated CO_2, as detailed in earlier studies [24].
- Role of argon: Argon, as an inert monatomic gas, undergoes ionization to sustain the arc and stabilize the plasma plume, providing the thermal bulk that drives the CO_2 dissociation without consuming the reactive oxygen species [24].

Consequently, the stream exiting the torch model (PLASCORE) is not merely a hot gas; it is a radical-rich, chemically active plasma plume. It correctly simulates the experimental condition where the feedstock is reacted with high-energy radicals rather than stable molecules, thereby significantly accelerating gasification kinetics. To accurately model the real-world thermal efficiency of the plasma torch, the model explicitly incorporates the energetic losses from the plasma core to its immediate surroundings before the plasma jet interacts with the feedstock. This thermal degradation is simulated using a secondary heat-loss block (ELECLOSS) and is attributed to two primary mechanisms:

- Electron recombination and quenching: As the highly ionized plasma jet expands and interacts with the surrounding atmosphere, high-energy electrons are lost to the cooler boundaries. The subsequent recombination of ions and quenching of the plasma plume led to a significant, unavoidable dissipation of thermal energy.
- Electrode sublimation: The intense, localized heat of the arc core at the cathode/anode attachment points drives the sublimation of the carbon/graphite electrodes. This endothermic phase change consumes a measurable portion of the supplied electrical energy. To account for this, a solid carbon feed (ELECTROD) is integrated into the torch model, accurately capturing both the physical material consumption and its

corresponding thermodynamic demands. The Ar-CO_2 thermal arc plasma generation model is shown in Figure 2.

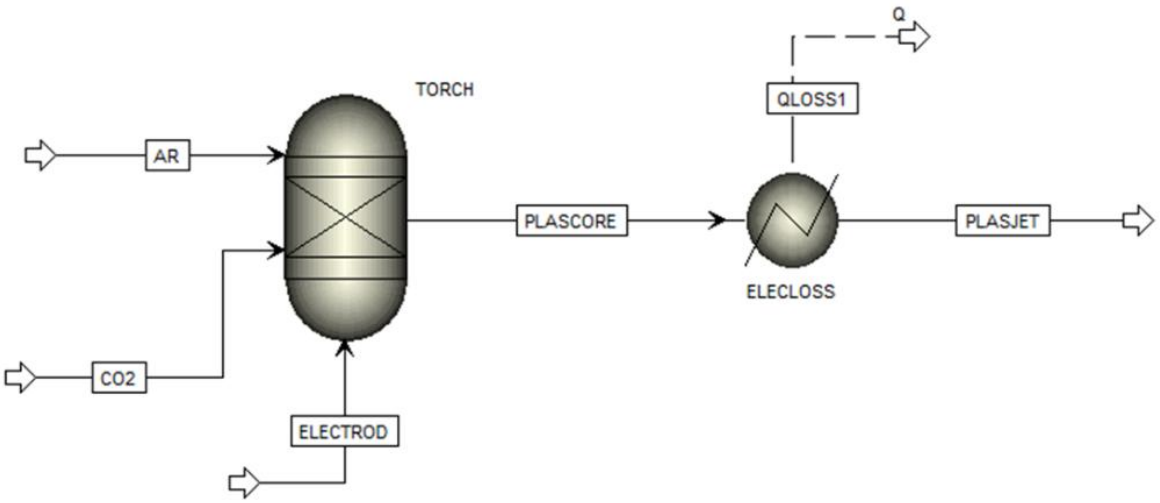

Figure 2. Ar-CO_2 thermal arc plasma generation model considering quenching properties of thermal plasma.

2.3.1.1 Microscopic characteristics of Ar-CO_2 thermal arc plasma

To accurately validate the assertion regarding the plasma core temperature localized between the electrodes, a study of plasma parameters viz. electron temperature (T_e) and electron density (n_e) is imperative. The energy imparted through the DC source is linked to the instantaneous kinetic energy of electrons in the thermal arc plasma, establishing a high-energy environment localized between the electrodes. The core region serves as an abundant source of energetic electrons, which drive diverse elementary collisional processes such as the electron-impact ionization of argon and the rotational-vibrational transitions of CO_2. These high-energy electrons further facilitate the population of various electronic excitation levels and the opening of specific dissociation channels for CO_2 [43,44]. Figure 3(a) shows different transitions of $CO_2^+(A^2\Pi - X^2\Pi)$, $CO^+(B^2\Sigma - X^2\Sigma)$ and $CO(d^3\Delta - a^3\Pi)$, Ar I, Ar II lines, $O^\bullet$ radical and occurrence of H_α trace impurities of water vapour measured in front of the core region using OES at the optimized conditions provides evidence of the above-mentioned collisional processes. The detailed kinetic mechanism and dissociation pathways are well explained in earlier study [24].

T_e and n_e are commonly used metrics to denote properties of plasmas. Both parameters are derived through the emission characteristics of Ar-CO_2 thermal plasma. Boltzmann plot technique is employed for estimation of T_e using the Equation 8 [45].

$$ln\left(\frac{I.\lambda}{A_q.g_q}\right) = \ln(hcN_p) - \frac{1}{k_B T_e} E_q \quad (8)$$

Where I: emission intensity, λ: transition wavelength, A_q: Einstein coefficient in upper state g_q: statistical weight in the upper state, E_q: Energy level of upper state of Ar I, and N_p: lower state level population. The subscript q denotes upper state level. Six Ar I lines were chosen from 696 – 912 nm as shown in Figure 3(b). The product of $A_q.g_q$ and E_q values corresponding to the Ar I lines is taken from national institute of standards and technology (NIST) database. From the above equation, the slope of linear fit profile of $ln\left(\frac{I.\lambda}{A_q.g_q}\right)$ vs E_q will be equivalent to the inverse of T_e.

For optimized conditions of Ar-CO_2 flow, the slope derived is 1.136 (as shown in Figure 3(b)) which translates to a value $T_e \approx 0.88$ eV corresponds to 10,208 K at the core plasma between the graphite electrodes. The obtained T_e agrees with other's salient work on thermal plasma using OES [46]. This supports the hypothesis of plasma core exceeding 8000 K. The estimation of n_e is achieved by performing a Voigt profile fitting of the H_α line at 656 nm, as shown in Figure 3(c). In atmospheric pressure plasmas, Stark broadening is one of the dominant broadening mechanisms because the high frequency of charged particle collisions generates intense local micro-fields that perturb the atomic energy levels. The FWHM ($\Delta\lambda_s$) value obtained from Voigt fitting is substituted in the empirical Equation 9 [47].

$$n_e = \left(\frac{\Delta\lambda_s}{1.78}\right)^{1.5} \times 10^{23}\ \mathrm{m}^{-3} \quad (9)$$

Where, $\Delta\lambda_s$ is stark broadening of H_α line with length scales in nm. The FWHM of Lorentzian component of H_α line found is $\Delta\lambda_s =$ 1.44 nm. This yields a $n_e = 7.27 \times 10^{22}\ m^{-3}$. At ambient conditions, the neutral particle density is in order of $n_o = 2.45 \times 10^{25}\ m^{-3}$ using $P = n_o k_b T_a$ where k_b is Boltzmann constant and T_a = 300 K. The ionization degree ($\alpha = \frac{n_e}{n_o}$) which is defined as the ratio of number density of ionized particles to total available neutral number density in the given region of plasma formation. Using the above n_e & n_o, $\alpha = 2.96 \times 10^{-3}$ is obtained which lies in close range for thermal plasma condition [46]. Thus, both plasma parameters obtained through OES provide an overview of conditions at the core region. This forms basis for the assumptions made regarding process methodology in ASPEN PLUS Modelling.

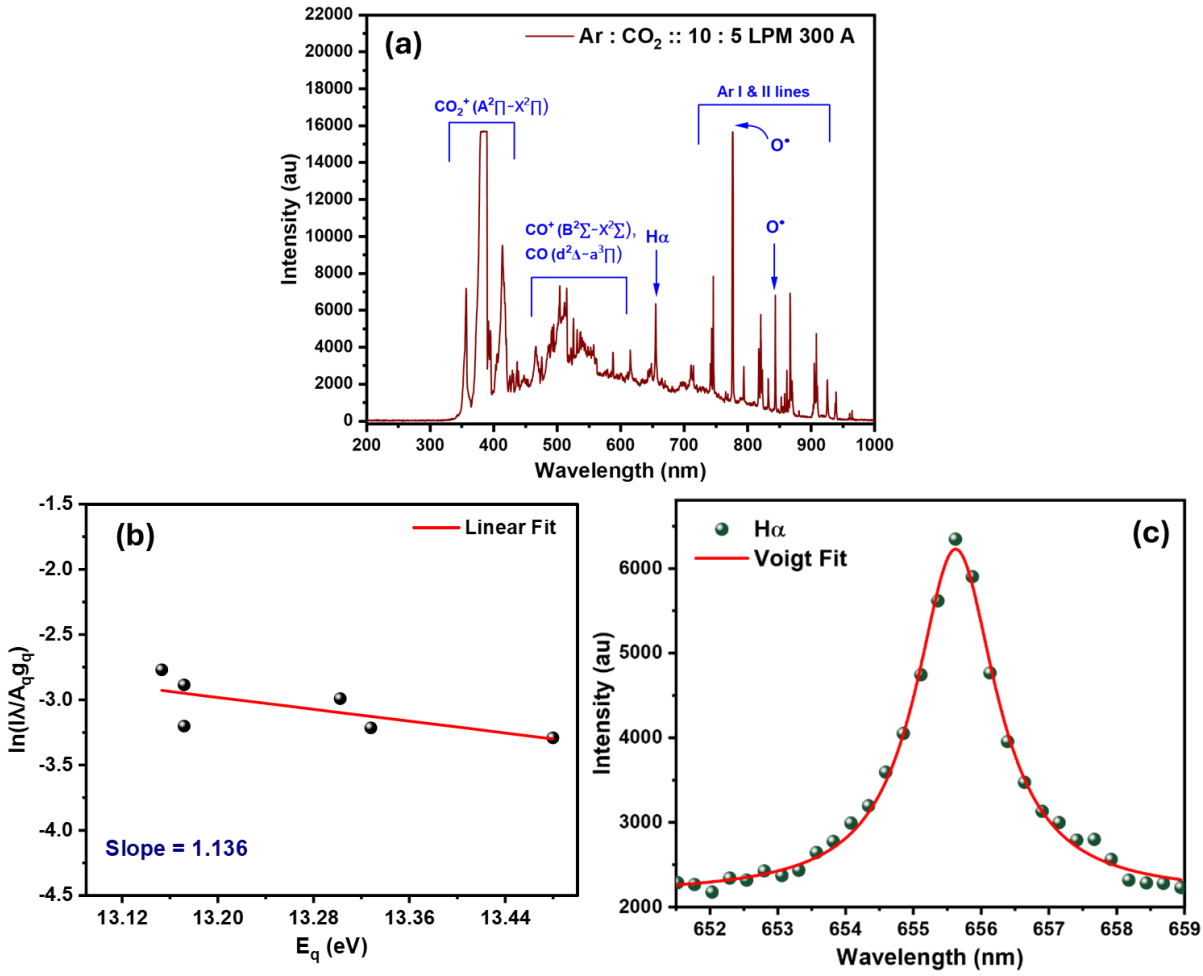

Figure 3. (a) Optical emission characteristics of Ar-CO_2 plasma formed between graphite electrodes (b) Boltzmann plot technique for estimation of electron temperature in Ar-CO_2 plasma using linear fit of $ln\left(\frac{I.\lambda}{A_q.g_q}\right)$ vs E_q using Ar I lines (c) Voigt fit for extracting line broadening of H_α at 656 nm in Ar-CO_2 plasma for determination of electron density.

2.4.2 Plasma gasification modelling

ASPEN PLUS does not have a dedicated unit operation for a plasma gasifier. The complex physical and chemical phenomena of the plasma reactor were modelled using a network of interconnected reactor blocks. The model is conceptually divided into three main stages: feedstock decomposition, high temperature zone (HTZ)/primary plasma plume zone, and the low temperature zone (LTZ)/secondary thermal gradient zone.

- Feedstock decomposition: The non-conventional LDPE feed is first directed into an RYield reactor (DECOMP). In this block, the polymer is broken down into its elemental constituents (C, H, O, N, S, and ash) according to the specified ultimate analysis. The

heat required for this endothermic devolatilization is provided by integrating the recovered heat from the downstream syngas cooling stage.

- HTZ: The elements from the decomposition block enter the primary gasification zone, modelled as an RGibbs reactor. This zone simulates the immediate vicinity of the plasma plume where temperatures exceed 2000 °C. The reactor operates by minimizing the total Gibbs free energy of the system to determine the equilibrium phase and composition. The thermal energy required to sustain this zone is supplied by the simulated plasma torch, using Argon as the plasma-forming gas.
- LTZ: To capture the steep spatial temperature gradients characteristic of plasma chamber, a secondary RGibbs reactor (LTZ) is placed immediately downstream of the HTZ. Modelled as an adiabatic reactor, this zone simulates the tail-flame region where the gas rapidly cools. This configuration successfully captures the occurrence of localized, highly exothermic recombination reactions such as methanation and the water-gas shift reaction, which govern the final syngas composition exiting the plasma chamber. The ASPEN PLUS model reactor, along with various streams, is shown in Figure 4.

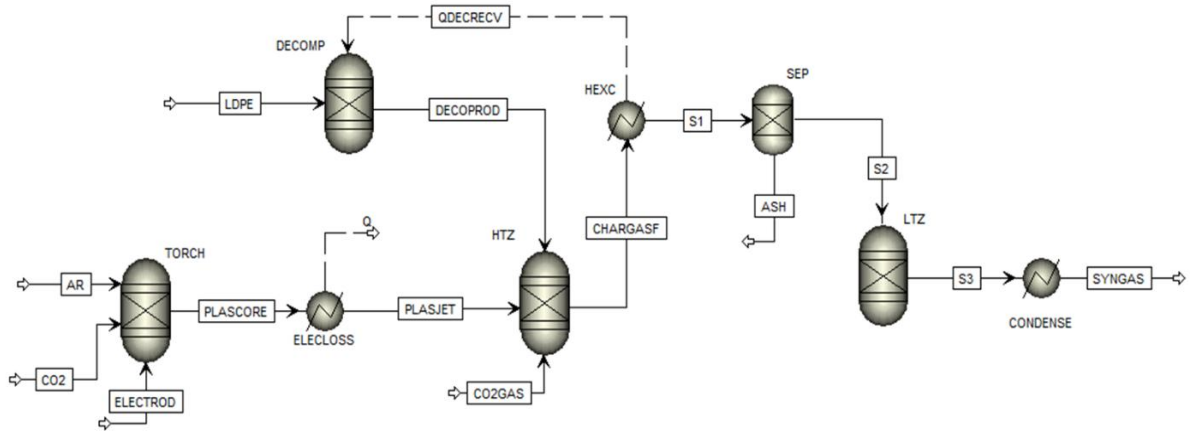

Figure 4. ASPEN PLUS model of Ar-CO_2 thermal arc plasma assisted CO_2 plasma gasification for LDPE plastic waste to energy.

2.4.3 Model assumptions

To establish a robust and solvable steady-state simulation, the following fundamental assumptions were incorporated into the model:

- The overall process operates under steady-state and steady-flow conditions.

- The gasification reactions occurring in the HTZ proceed fast enough to achieve complete thermodynamic equilibrium, a valid assumption given the extreme temperatures generated by the plasma torch.
- The complex fluid dynamics and transport phenomena within the plasma chamber are simplified, focusing exclusively on the thermodynamic limits of the chemical conversions.
- Pressure drops across the reactor blocks are considered negligible.
- All heat losses from the secondary thermal zone/lower temperature zone (LTZ) to the environment are assumed to be zero (adiabatic operation), allowing temperature fluctuations to be driven entirely by the internal enthalpy changes of the localized reactions.
- The ash content of the LDPE feed is treated as chemically inert and is separated from the gas phase without interacting with the primary syngas components.

2.4.4 Model limitations

Although these two-zone models significantly improve the representation of plasma gasification by incorporating realistic plasma generation and heat-loss mechanisms, it is vital to acknowledge the inherent boundaries of macroscopic thermodynamic simulation. Specifically, the model calculates maximum theoretical yields based on thermodynamic equilibrium, which does not explicitly resolve the complex micro-kinetics or the exceptionally short residence times characteristic of physical plasma reactors. Furthermore, as a zero-dimensional simulator utilizing the Local Thermodynamic Equilibrium (LTE) assumption, the software effectively approximates the complex three-dimensional magnetohydrodynamics and continuous spatial temperature gradients into discrete reactor blocks. Despite these standard simplifications, the developed model successfully captures the critical thermodynamic limits and provides a highly robust framework for evaluating the plasma gasification performance.

3 Results and discussion

This section presents a comprehensive evaluation of the experimental and theoretical findings from the thermal arc plasma gasification of LDPE waste. It begins by establishing the optimal operating conditions through an analysis of plasma plume dynamics and chamber preheating stability under various carrier gas environments. The predictive accuracy of the developed ASPEN PLUS thermodynamic model is then validated against in-house thermal plasma gasification system. Building on this validated baseline, the study predicts the

gasification performance utilizing steam and a steam-CO_2 mixed agent to optimize syngas and hydrogen yields. A detailed comparative assessment was subsequently performed across these optimal scenarios, analyzing critical operational metrics, including SSY, LHV, CGE, and CCE. Finally, the industrial viability of the proposed technology was established through a rigorous environmental performance analysis incorporating carbon footprint benchmarking and carbon capture and utilization (CCU) mass balances for net-zero processing, coupled with a preliminary techno-economic projection of specific energy consumption (SEC) for pilot-scale commercialization within the hydrogen economy.

3.1 Feedstock

The proximate analysis showed very low moisture (0.15 %) and ash content (4.76 %), along with a high volatile matter (94.48 %) and low fixed carbon (0.61 %). The ultimate analysis revealed a high carbon content of 73.40%, hydrogen content of 12.30 %, negligible nitrogen (0.02 %) and sulfur (0.49 %), and oxygen content of 9.03 %. The high carbon and hydrogen contents confirm the strong energy recovery potential of LDPE plastic waste. Based on these results, the feedstock satisfies the Indian central pollution control board (CPCB) guidelines for waste-to-energy applications, including volatile matter greater than 45 %, calorific value exceeding 5.77 MJ/kg (1200 kcal/kg), fixed carbon less than 15 %, and total inert content below 35 % [48]. The high volatile content and calorific value make LDPE plastic waste highly suitable for plasma gasification and syngas production. The results of the proximate and ultimate analyses are presented in Table 1.

Table 1: Proximate & ultimate analysis of the feedstock

Parameters	**Value**	**Test methods standards**	**Standards reference**
Proximate analysis			
Moisture content (%)	0.15	IS: 1350 (P-1) 1984	[49]
Volatile matter (%)	94.48	IS: 1350 (P-1) 1984	
Ash content (%)	4.76	IS: 1350 (P-1) 1984	
Fixed carbon (%)	0.61	IS: 1350 (P-1) 1984	
Ultimate analysis			
Carbon (%)	73.40	IS: 1350 (P-4/Sec-1) 1974	[50]
Hydrogen (%)	12.30	IS: 1350 (P-4/Sec-1) 1974	
Nitrogen (%)	0.02	IS: 1350 (P-4/Sec-2) 1999	[51]
Sulfur (%)	0.49	IS: 1350 (P-3) 1969	[52]

Table 1: Proximate & ultimate analysis of the feedstock

Parameters	Value	Test methods standards	Standards reference
Oxygen (%)	9.03	By calculation	
Calorific value			
High calorific value (MJ/kg)	40.80	IS: 1350 (P-2) 1975	[53]
Low calorific value (MJ/kg)	38.10	IS: 1350 (P-2) 1975	

3.2 Preheating study of the plasma chamber, along with plasma plume dynamics

Preheating of the plasma chamber was studied experimentally for an hour to reduce the risk of toxic gas release during waste processing at lower temperatures. Here, preheating depends solely on the thermal plasma arc and its plume dynamics. The generation and stability of thermal arc plasma are strongly influenced by the choice of carrier gas, which governs ionization characteristics, plume morphology, heat transfer, and electrode behavior. In the present study, Ar, CO_2, and Ar-CO_2 mixtures were systematically evaluated to identify the most suitable plasma-forming environment for subsequent waste processing.

Argon plasma served as the reference case due to its monoatomic and electropositive nature. Owing to its low ionization energy and absence of electron attachment mechanisms, argons readily form a stable, vertically aligned plasma column with uniform intensity. At an optimized flow rate of 15 LPM and a current supply of 300 A, argon plasma achieved the target preheating temperature of 850 °C within 16 minutes, consuming approximately 1.95 kWh of energy. High-speed imaging revealed a well-defined plume extending approximately 20 ± 3 cm in length with a diameter of about 2 ± 0.2 cm at 300 A, exhibiting stable arc-root attachment and minimal fragmentation. The quasi-neutrality of argon plasma, maintained through radiative and three-body recombination processes, ensures sustained electron density and uniform heat transfer. The details of argon thermal arc plasma generation and its high-speed images for the following conditions are presented in detail in earlier studies [19]. However, while argon plasma demonstrated excellent thermal stability, being an inert gas, it functions primarily as a thermal medium rather than a chemically reactive environment. Thus, further experiments were conducted using CO_2 as a carrier gas for thermal arc plasma generation. CO_2 plasma exhibited markedly different behavior. Due to its molecular and electronegative nature, CO_2 introduces significant electron attachment and dissociative recombination, depleting free electrons and destabilizing the discharge. High-speed visualization showed plume inclination, fragmentation,

and reduced intensity compared to argon plasma. Even at 15 LPM and 300 A, the maximum chamber temperature reached only ~800 °C, failing to meet the required preheating threshold. The plume length (~15 ± 2 cm) decreased over time due to fragmentation, and localized constriction between electrodes intensified carbon ablation. The instability arises from several coupled effects: enhanced electron loss through dissociative attachment ($e^- + CO_2 \rightarrow CO + O^-$), formation of negative ions causing ionic wind, thickened cathode sheath reducing thermionic emission, and vortex-induced perturbations from electrode surface cavities [54,55]. Although CO_2 plasma inherently offers the advantage of reactive participation in gas-phase chemistry, its unstable discharge characteristics limit its direct applicability as a standalone plasma-forming gas. The details of fragmentation and inclination at various flow rates are already reported in earlier study [24].

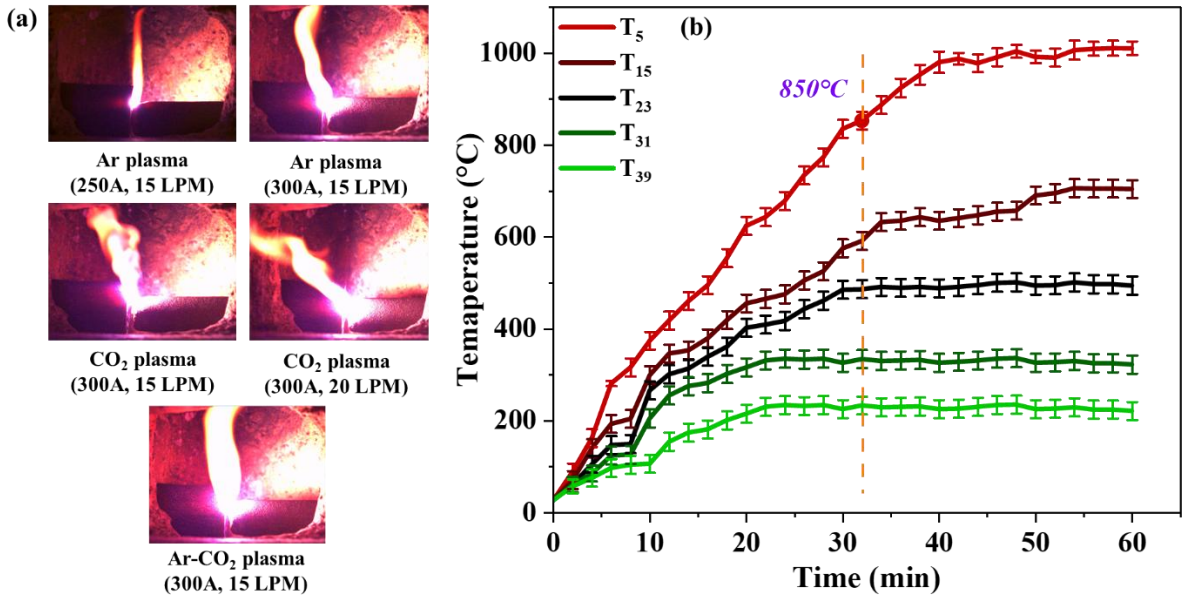

Figure 5. (a) High-speed imaging analysis of thermal arc plasma of various carrier gases and (b) preheating temperature study for optimized Ar-CO_2 thermal arc plasma.

To overcome these limitations, a mixed-gas plasma using argon and CO_2 was investigated. At 250A with a 10 LPM Ar and 5 LPM CO_2 mixture, the plasma exhibited better uniformity than pure CO_2 but could not reach 850 °C. Increasing the current to 300A stabilized the plume and improved energy transfer. The resulting plasma showed a maximum plume length of 25±3 cm and diameter of 3±0.3 cm, achieving 850 °C within 32 minutes at an energy input of 5.6 kWh. Further, increasing the CO_2 proportion to 10 LPM resulted in plume fragmentation and severe electrode erosion. Therefore, the optimized preheating condition was established as an Ar-CO_2 mixture of 10 LPM argon and 5 LPM CO_2 at 300A. This configuration provided stable

plasma behavior, reduced electrode wear, and sufficient thermal energy to achieve the desired preheating temperature before initiating the waste feeding. The details of the high-speed images and the preheating plasma chamber temperature plot are given in Figure 5 (a) and (b) respectively.

3.3 Plasma gasification modelling study analysis

The simulation of the plasma gasification process was anchored to the optimized experimental parameters established during the steady-state plasma generation phase. To simulate stable thermal arc formation, the baseline electrical input was set to 300 A and 25 V. The carrier gas feed rates introduced into the torch model (TORCH) were directly imported from the experiment performed with an Ar flow of 10 LPM (0.978 kg/h) and a CO_2 flow of 5 LPM (0.54 kg/h). A critical parameter in the ASPEN PLUS model is the primary gasification temperature within the High-Temperature Zone (HTZ). In the physical reactor, steep spatial temperature gradients exist between the arc core and the chamber walls. During the experiments, visual observation of graphite electrode degradation indicated that the outer layer of the plasma plume surpassed the sublimation point of graphite (approximately 3400 °C), suggesting localized temperatures in the range of 3000−4000 °C near the electrodes. Conversely, the thermocouple (T_5) situated at the inner refractory wall adjacent to the plasma zone recorded bulk temperatures exceeding 1000 °C. To accurately represent the macro-level thermodynamic environment where the primary gasification reactions reach equilibrium, an average effective gasification temperature of 2000 °C was established for the HTZ. Accordingly, the thermal dissipation from the ultra-high-temperature plasma core was calculated to meet this 2000 °C target. This thermal penalty was integrated into the model via the ELECLOSS block, which explicitly simulates the heat loss between the initial plasma generation (PLASCORE stream) and the expanding plasma jet (PLASJET stream) before it interacts with the feedstock.

Following the establishment of this baseline plasma model, a sensitivity analysis was conducted to evaluate the thermodynamic limits and syngas composition resulting from the Ar-CO_2 plasma-driven conversion of LDPE waste. Specifically, the study investigated the influence of introducing an additional CO_2 gasification agent stream into the HTZ, with its mass flow rate varying from zero to 5 kg/h. The simulation evaluated the equilibrium composition in both mass flow rate (kg/h) and volume fraction (vol%), capturing the complex interplay of thermal cracking, dry reforming, and localized recombination reactions. The trends

observed can be distinctly categorized into three operational phases: plasma pyrolysis (under-oxidation), optimal syngas production, and syngas dilution (over-oxidation).

Initially, in the absence of additional CO_2 (gasification agent), the system operates around pyrolysis conditions, yielding approximately 0.217 kg/h of solid carbon (char) and a syngas dominated by CH_4 at nearly 49.6 vol%. As CO_2 is incrementally introduced (zero to 1.5 kg/h), the high-enthalpy plasma environment promotes two primary endothermic pathways: the Boudouard reaction aggressively consumes the solid carbon to form carbon monoxide (CO), and the dry reforming of methane cracks the light hydrocarbons. This is visually corroborated by the sharp, linear decline in both solid carbon mass and CH_4 volume fraction (49.6 % to ~15 %), accompanied by a steep, proportional rise in both CO and H_2 production. During this phase, virtually all injected CO_2 is consumed, maintaining the residual CO_2 volume in the product gas at near-zero levels.

The critical operational threshold is reached at a CO_2 flow rate of approximately 1.75 kg/h. At this specific stoichiometric point, approximately all the solid carbon is consumed, indicating a near-complete carbon conversion efficiency. Consequently, the production of combustible gases reaches its optimal peak. The hydrogen fraction hits its maximum value of 22.18 vol% (0.066 kg/h), and the carbon monoxide fraction stabilizes near its peak at 66.59 vol% (2.82 kg/h). The methane fraction is simultaneously minimized to 8.78 vol%. At this optimal operating point, the syngas purity (H_2 & CO) exceeds 88 vol%, making it highly calorific and ideal for downstream energy recovery or chemical synthesis.

Increasing the CO_2 flow rate beyond the stoichiometric optimum of 1.75 kg/h yields diminishing returns and degrades the syngas quality. Because the solid carbon has already been completely consumed, the excess CO_2 has no carbon left to gasify via the Boudouard reaction. Instead, the unreacted CO_2 begins to pass through the reactor system, acting as a thermal diluent. This is clearly evidenced by the linear surge in CO_2 concentration in the final gas stream, which climbs rapidly to approximately 34.8 vol% at a 5 kg/h feed rate. Consequently, the overall volume percentage of both CO and H_2 decreases due to the compounding effects of chemical consumption and volumetric dilution by the unreacted carbon dioxide. Detailed sensitive analysis is shown in Figure 6, where the syngas composition is separately shown in kg/h in Figure 6(a) to showcase the char production at initial stages whereas Figure 6(b) shows composition by vol%.

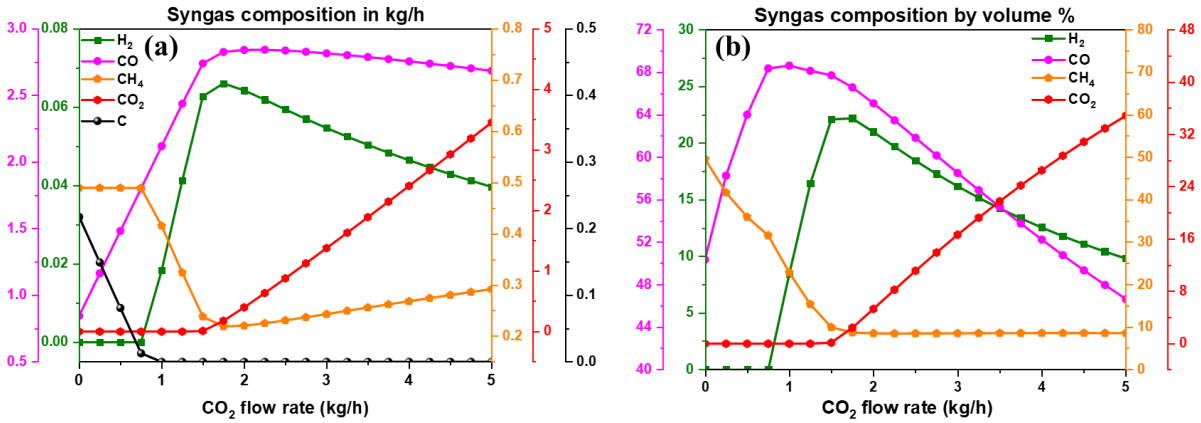

Figure 6. The sensitivity analysis for CO_2 as a gasification agent for variation in syngas (a) in kg/h and (b) by volume %.

3.4 Model validation with experimental data

The predictive accuracy of the thermodynamic model was experimentally validated using Ar-CO_2 thermal arc plasma generation in a plasma chamber. After successfully preheating the plasma chamber to 850 °C, LDPE waste feeding was initiated. Simultaneously, CO_2 was continuously introduced into the chamber at a flow rate of 14 LPM (1.5 kg/h, model-generated optimal syngas production condition) as the primary gasification agent alongside the thermal plasma plume. The waste was processed at a nominal feed rate of 1 kg/h. However, to prevent the rapid gas evolution, subsequent over-pressurization, and potential gas leakages from the chamber (observed during continuous feeding), the material was introduced via the screw feeder in discrete, controlled batches of 80 g every 3 minutes. This intermittent feeding strategy successfully maintained a steady gas production rate and stabilized the internal pressure of the plasma chamber.

The experimental analysis yielded a syngas composition by vol% of approximately 21 % H_2, 63 % CO, 10 % CH_4, and 6 % CO_2. These empirical results demonstrate a strong correlation with ASPEN PLUS thermodynamic predictions. The model predicted an H_2 concentration of 22.18 vol%, CO concentration of 67.72 vol%, and CH_4 of 10.01 vol.%, which are in excellent agreement with the experimental data. The variations observed for the specific presence of 6 % CO_2 vs. the model's ~0.16 % can be readily attributed to the inherent kinetic limitations of the physical reactor. While the ASPEN PLUS model calculates maximum theoretical yields based on perfect thermodynamic equilibrium, the extremely rapid transit of gases through the high-temperature gradient zones in the physical plasma chamber prevents the complete dry reforming of all methane. It limits the absolute completion of the Boudouard reaction.

Nevertheless, the high degree of parity between the theoretical model and the experimental data strongly validates the chosen two-zone (HTZ and LTZ) simulation approach. A similar observation of the composition of syngas from mixed plastic waste (with similar waste characteristics) processing was reported by Tamošiūnas et al. [31]. The results are in strong collaboration with the modelling study conducted for LDPE waste. It suggests that incorporating realistic plasma-generation parameters and discrete thermal-gradient zones provides a highly reliable framework for predicting syngas quality and scaling Ar-CO_2 plasma gasification systems. The details of the model validation study using experimental data are given in Table 2.

Table 2. Validation of the LDPE plasma gasification model

Gas Component	Exp. (vol%)	Model (vol%)	Rel. Error (%)	Tamošiūnas et al. [31]	Rel. Error (%)
H_2	21.0	22.1	5.24	22	4.76
CO	63.0	67.7	7.46	55	12.69
CH_4	10	10.0	0.00	7	30.00*
CO_2	6.0	0.16	97.33*	7	16.66

*The high relative error (97.33 %) for CO_2 is an expected artifact of comparing a kinetic-limited physical process to a perfect thermodynamic equilibrium model. Because the physical reactor does not allow infinite residence time, the endothermic boudouard and reforming reactions do not reach 100 % completion, leaving approximately 6.0 % unreacted CO_2 compared to the model's idealized 0.16 %. This unreacted CO_2 directly accounts for the slightly lower experimental yields of H_2 and CO. Similarly, for Tamošiūnas et al., there is a higher relative error for CH_4 as C_2H_4 at 3 vol% was reported, which is not observed in the current experimental results; hence, the CH_4 percentage volume is lower comparatively.

3.5 Prediction of syngas yield with the addition of steam and mixed gasification agent

To evaluate the potential to optimize H_2 yield from LDPE waste, a subsequent simulation was conducted using steam as the primary gasification agent instead of CO_2. The ASPEN PLUS model was modified to inject a variable steam stream, while maintaining the baseline Ar-CO_2 thermal arc plasma carrier gas (10 LPM Ar and 5 LPM CO_2) shown in Figure 7(a). A sensitivity analysis was performed by varying the steam flow rate from zero to 3 kg/h, corresponding to a steam-to-feed (S/F) mass ratio of zero to 3. The resulting equilibrium composition (in kg/h and vol%) shown in Figure 7(b) and 7(c) respectively reveals a distinctly different thermochemical pathway compared to CO_2 gasification, driven by the strong affinity of steam for donating hydrogen.

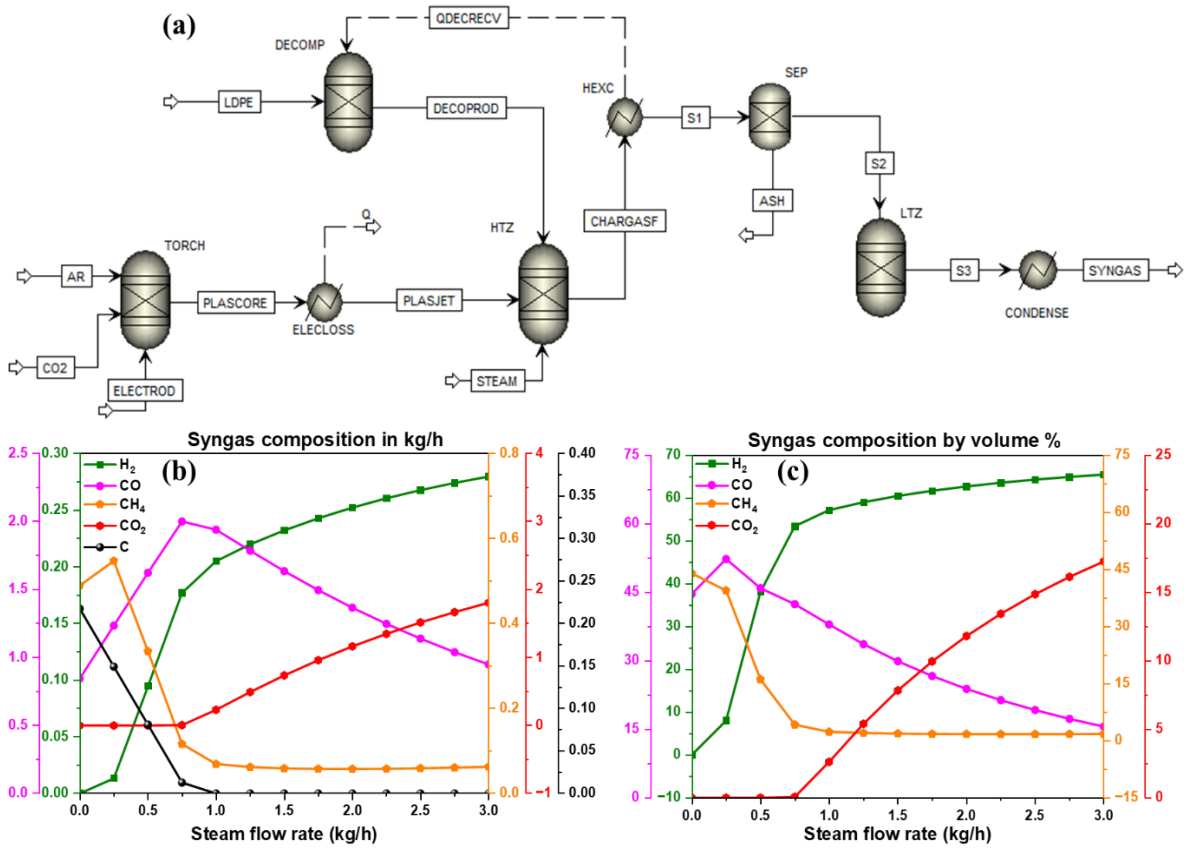

Figure 7. (a) Model used for steam plasma gasification, and (b) sensitivity analysis for steam as a gasification agent for variation in syngas and gas composition in kg/h and (c) by volume %.

Initially, in the absence of an additional gasification agent, the system operates without any external steam addition. The only gasifying agent present is the 0.54 kg/h of CO_2 introduced via the Ar-CO_2 carrier gas. The limited supply of gasification agent, resulting in a baseline state identical to the previous CO_2 study: a significant yield of char (0.217 kg/h) and product gas dominated by CH_4 (~43.9 vol%) and CO (~44.6 vol%), with negligible H_2 production. As steam is incrementally introduced up to 1.0 kg/h, it acts as a highly aggressive oxidant and hydrogen donor. The extreme thermal environment of the plasma plume triggers two dominant endothermic reactions. First, the heterogeneous water-gas reaction ($C + H_2O \rightleftharpoons CO + H_2$) rapidly consumes solid carbon soot. Second, steam methane reforming (SMR) ($CH_4 + H_2O \rightleftharpoons CO + 3H_2$) aggressively cracks the highly concentrated methane. This is evident in Figure 7(b), where the precipitous drop in both the solid carbon and CH_4 volume fractions (falling from ~43.9 % to just 2.3 %) is shown. Correspondingly, the H_2 volume fraction surges dramatically, crossing the 50 % mark before reaching 1.0 kg/h. The stoichiometric optimum for balanced syngas production is achieved at a steam flow rate of approximately 1.0 kg/h (an S/F ratio of

1.0). At this point, solid carbon is completely depleted, indicating near-complete carbon conversion. The resulting syngas achieves their highest combined purity, consisting of 57.14 vol% H_2 and 37.93 vol% CO. Residual CH_4 is minimized to 2.31 vol%, and CO_2 is 2.61 vol%. Increasing the steam flow rate beyond 1.0 kg/h fundamentally alters the gas composition due to the water-gas shift (WGS) reaction ($CO + H_2O \rightleftharpoons CO_2 + H_2$). Because the solid carbon is already fully consumed, excess steam reacts directly with the carbon monoxide generated in the previous phase. This shift is clearly visible in the data curves as steam increases from 1.0 to 3.0 kg/h, the CO fraction steadily plummets from 37.93 vol% down to 15.57 vol%. Concurrently, the CO_2 fraction rises sharply from negligible quantity to 17.24 vol%. While this WGS pathway continues to boost H_2 yield (reaching 65.43 vol% at 3 kg/h), it brings down the syngas calorific value by replacing combustible CO with CO_2.

While the theoretical potential of steam plasma gasification is highly promising, the studies on plastic waste gasification, particularly using Ar-CO_2 thermal arcs with graphite electrodes, remain underexplored. Consequently, to establish a reliable baseline and validate the predictive accuracy, the simulation results were compared with a study on steam plasma gasification of polyethylene (PE) waste conducted by Park et al. [56]. This preliminary validation is conducted to ensure the model provides a robust foundation for upcoming experimental studies on graphite electrode-based Ar-CO_2 plasma-assisted steam gasification of plastic waste. In the referenced experimental study, a V-type plasma torch was utilized to completely decompose PE into low-molecular-weight gases. The literature reported that at a steam-to-PE mass ratio of 1.2, the system produced a highly calorific syngas, with approximately 65.0 vol% H_2 and 30.0 vol% CO. To validate the ASPEN PLUS model against these findings, the simulation data at the closest equivalent operating point, a steam feed rate of 1.25 kg/h (representing a S/F ratio of 1.25), were studied for comparison. At this specific condition, the model predicted a syngas composition of 59.0 vol% H_2 and 33.6 vol% CO. The comparison between the literature data and the model simulation reveals a strong predictive alignment, successfully capturing the dominant shift toward hydrogen production when utilizing steam. The relative errors for the primary syngas constituents are well within an acceptable range for macroscopic thermodynamic modelling, as shown in Figure 8 (a).

The minor deviations between the model and the literature data (a slight under-prediction of H_2 and an over-prediction of CO) are physically consistent and expected. The referenced experiment used a pure-steam plasma system, whereas the developed model employs a mixed Ar-CO_2 carrier gas (0.54 kg/h of CO_2 and 0.978 kg/h of Ar) to imitate the specific graphite

electrode setup. The inclusion of this CO_2 in the carrier gas inherently shifts the equilibrium slightly, promoting additional CO formation via the boudouard reaction while slightly diluting the overall H_2 volume fraction. Overall, the strong correlation between the experimental benchmarks and the simulation validates the model's accuracy in predicting steam-driven gasification pathways. It provides high confidence in using this model to guide future physical experiments aimed at optimizing hydrogen yields from Ar-CO_2 plasma systems.

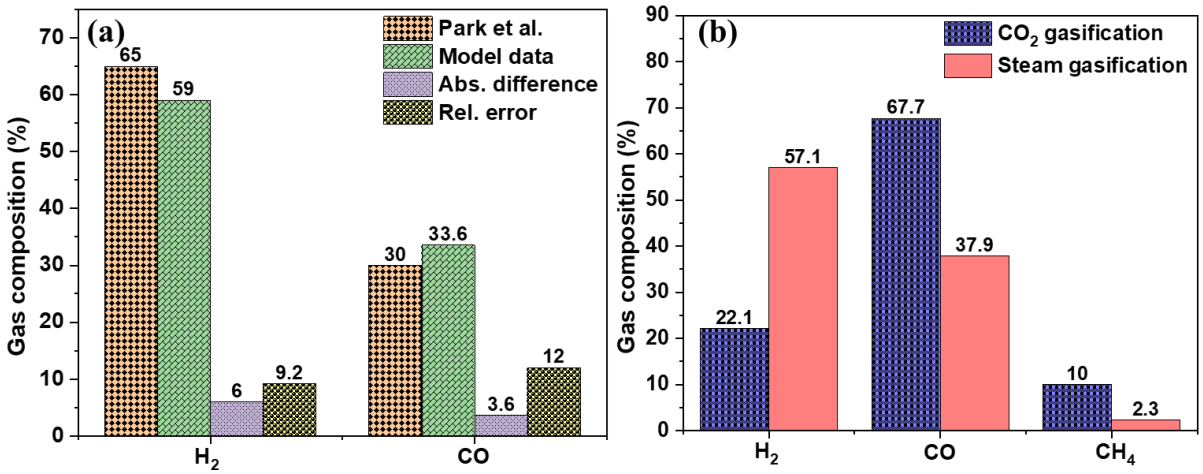

Figure 8. (a) Validation of the steam plasma gasification model with experimental data and (b) a comparison study of CO_2 plasma gasification and steam plasma gasification models for the prediction of syngas yield.

Comparing these results to the CO_2 gasification study (as mentioned in section 3.3) highlights a stark operational divergence. The detailed comparison study is given in Figure 8(b). Utilizing CO_2 as the gasification agent required a higher mass flow (1.75 kg/h) to achieve complete carbon conversion and produced a syngas heavily skewed toward carbon monoxide (H_2: 22.18 vol%, CO: 66.59 vol%). Whereas, steam gasification achieves complete carbon conversion at a much lower mass flow rate (1.0 kg/h) and fundamentally shifts the syngas profile, producing a hydrogen-rich gas (H_2: 57.14 vol%, CO: 37.93 vol%). Ultimately, the model demonstrates that Ar-CO_2 thermal plasma combined with steam injection is a highly efficient configuration for maximizing H_2 yields from plastic waste. However, strict control of the S/F ratio (optimally around 1.0) is essential to prevent the WGS reaction from over-oxidizing the syngas and generating excessive CO_2.

While utilizing steam as a gasification agent maximizes the hydrogen yield, it introduces both chemical and operational limitations. Chemically, as demonstrated in the previous section, excess steam shifts the thermodynamic equilibrium via the WGS reaction, which ultimately dilutes the product syngas with non-combustible CO_2 at the expense of valuable CO.

Operationally, managing steam as a primary feed gas is physically and economically more demanding than utilizing ambient-temperature gases such as nitrogen, air, or CO_2. Steam generation requires high temperature & high-pressure boiler systems, continuous heat loss management along the delivery lines to prevent condensation, and stringent safety precautions.

To avoid such challenges, a mixed gasification agent model approach using both steam and CO_2 was investigated as shown in Figure 9(a). Mixing these two agents offers a critical synergistic advantage: it significantly reduces the total steam flow rate required, thereby lowering operational costs and thermal management hurdles. Furthermore, the simultaneous injection of CO_2 counterbalances the adverse chemical effects of pure steam. By introducing an active carbon-oxygen source into the plasma environment, the equilibrium is strongly driven toward the endothermic boudouard and dry reforming reactions. This ensures a balanced, continuous production of CO to actively suppress the WGS reaction from over-oxidizing the syngas into CO_2. To pinpoint the optimum operating condition for this mixed gasification agent approach, a multiparameter sensitivity analysis was conducted in the ASPEN PLUS model. The flow rates of both the steam and CO_2 were varied simultaneously from 0 to 3 kg/h, and the resulting syngas equilibrium was evaluated to determine the optimal balance between high H_2 production, high CO retention, and minimal CO_2 dilution.

The contour data shown in Figure 9 reveals a highly dynamic interplay between the reforming and shift reactions across the 0 to 3 kg/h steam feed rate range. When both agents are supplied at higher flow rates (e.g., 2.0 to 3.0 kg/h each), the system quickly crosses into over-oxidation. For instance, at a feed of 2.0 kg/h CO_2 and 2.0 kg/h steam, the H_2 and CO yields drop to 47.0 vol% and 23.7 vol%, respectively, while the CO_2 fraction surges to over 25.7 vol%. This indicates that the combined oxygen load from both agents exceeds the available solid carbon, leading to severe thermal dilution. Thus, carefully metering the agents at lower flow rates unlocks highly synergistic operating points that surpass the pure-agent baselines:

- Balance condition (0.5 kg/h Steam + 0.5 kg/h CO_2): At this balanced feed rate, the system produces an exceptionally pure syngas consisting of 44.16 vol% H_2 (Figure 9(b)), and 49.99 vol% CO (Figure 9(c)), alongside 5.82 vol% CH_4 (Figure 9(d)). Most importantly, the CO_2 concentration is approximately eliminated (Figure 9(e)). This point yields an overall combustible syngas purity of 94.15 vol%. From an operational perspective, this is a significant breakthrough: it cuts the required steam usage in half (compared to the 1.0 kg/h pure-steam optimum) while preserving a high hydrogen yield

and reducing CO_2 to an insignificant level. However, as per the earlier discussion and experimental results, it is obvious that the CO_2 concentrations will not be as insignificant as modelling shows but will be on the lower side compared to pure gasification agents.

- The hydrogen-optimized condition (0.75 kg/h Steam + 0.25 kg/h CO_2): For applications that strictly prioritize hydrogen production while still minimizing steam load, a slightly steam-heavy mixture proves optimal. At this point, the H_2 yield reaches 51.96 vol%, CO remains strong at 43.65 vol%, and CO_2 stays extremely low at 1.18 vol%. This operating condition yields the highest combined syngas purity in the entire dataset at 95.61 vol% (H_2 + CO).

The theoretical data conclusively prove that mixing steam and CO_2 is superior to utilizing either agent in isolation. By supplying a low, controlled flow of CO_2 (0.25−0.5 kg/h) alongside a reduced steam feed (0.5−0.75 kg/h), the plasma gasifier efficiently cracks LDPE waste to produce a syngas with a purity exceeding 94 vol%. The optimum condition in case of mixed gasification agent is 0.75 kg/h of steam, and 0.25 kg/h of CO_2 leads to the production of highest possible pure syngas (H_2: 51.96 vol%, CO: 43.65 vol%, CH_4: 3.21 vol% and CO_2: 1.18 vol%) production for the given LDPE waste. This approach successfully resolves the dilemma of steam gasification: it drastically lowers the physical steam requirement, stabilizes the carbon monoxide yield, and chemically prevents the runaway formation of carbon dioxide.

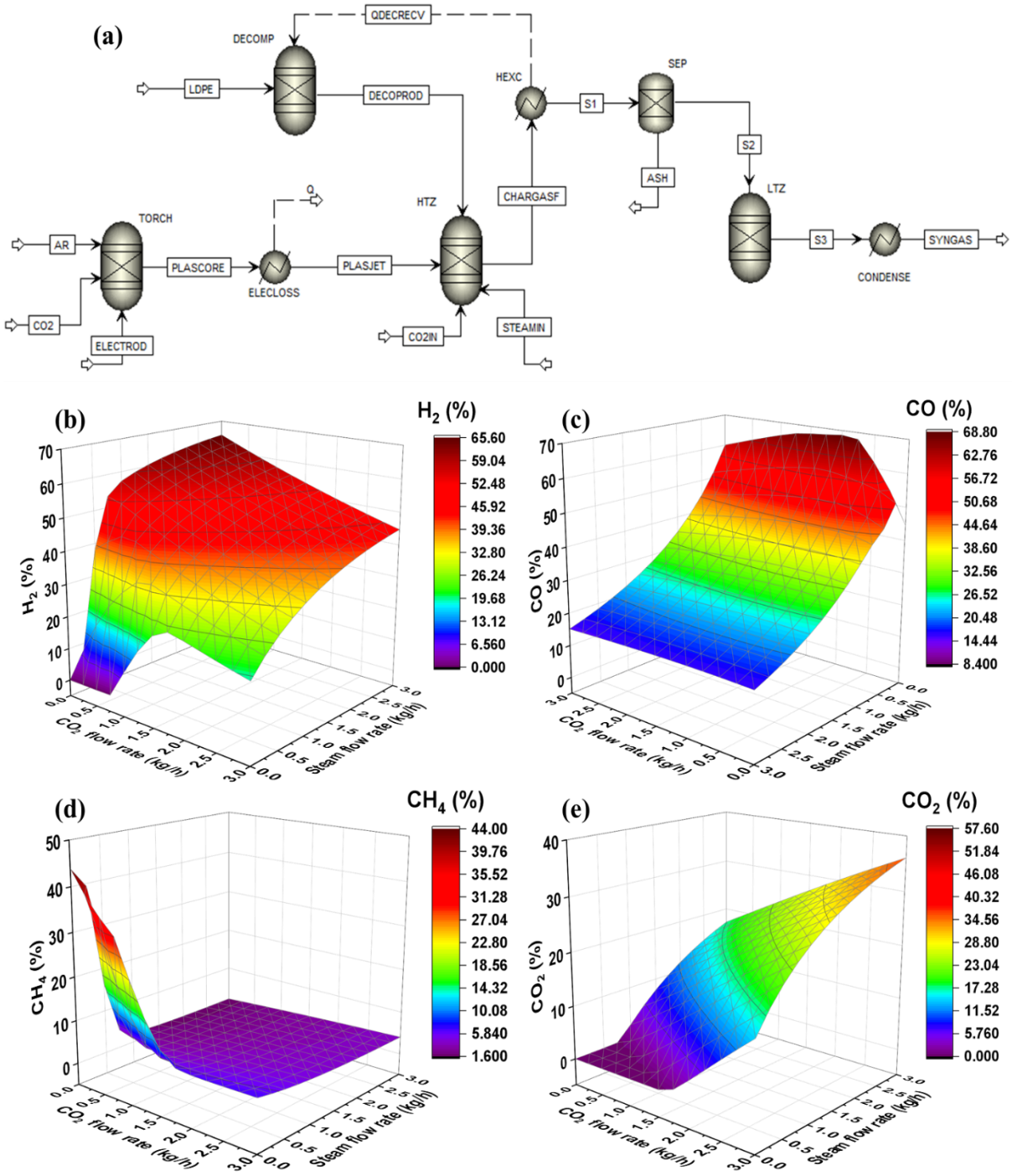

Figure 9. (a) ASPEN PLUS model for mixed steam and CO_2 plasma gasification, gas composition of (b) H_2, (c) CO (d) CH_4 and (e) CO_2 by volume % from variation of gasification agents of sensitivity analysis.

3.6 Plasma gasification reaction mechanism

Based on the optimized Model III conditions, the plasma gasification mechanism of LDPE is proposed as shown in Figure 10.

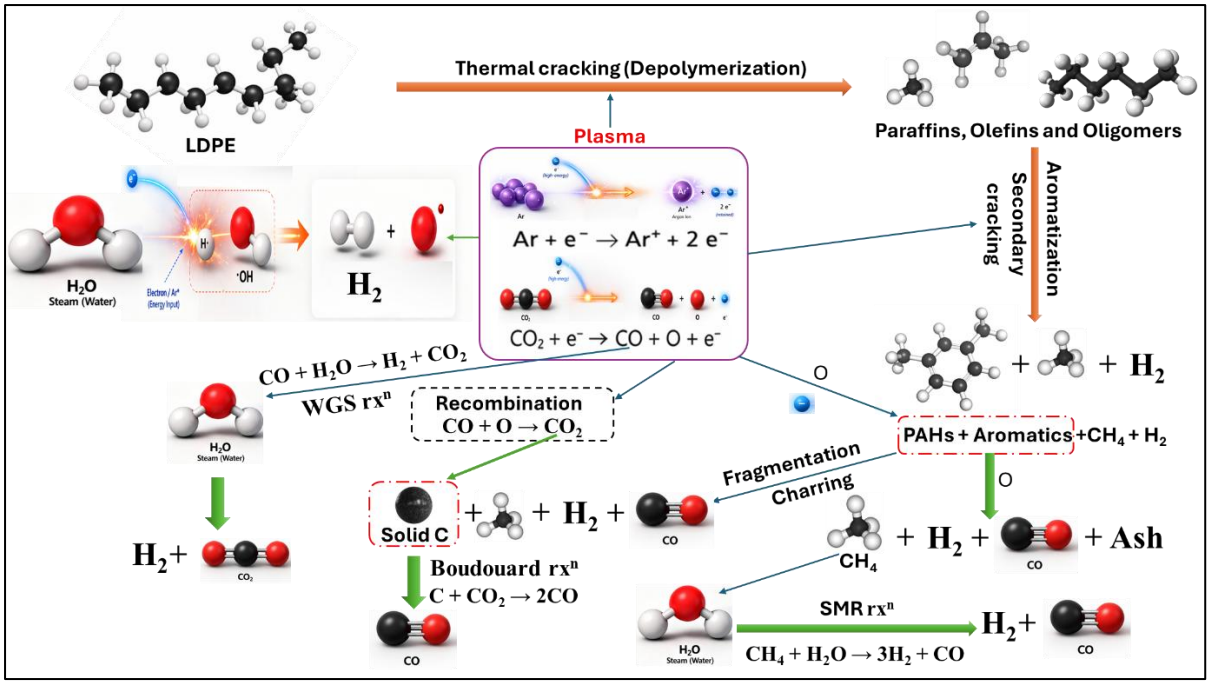

Figure 10. Thermo-chemical decomposition mechanism of LDPE in an Ar-CO_2 thermal plasma gasification process.

At initial stage, LDPE undergoes thermal cracking through random C–C bond scission under the high-temperature plasma environment. This process generates paraffins, olefins, and oligomeric hydrocarbons as primary products [57]. The unstable intermediates further undergo secondary cracking due to their high reactivity [58]. This leads to the formation of light hydrocarbons such as CH_4 along with smaller unsaturated species and H_2. The presence of unsaturated fragments promotes cyclization and aromatization reactions, resulting in the transient formation of poly aromatic hydrocarbons (PAHs) and aromatic intermediates [59]. However, these species do not accumulate due to the highly reactive plasma atmosphere. In the plasma zone, argon is ionized by electron impact to generate energetic electrons and excited species, which sustain the plasma and enhance reaction kinetics. Simultaneously, CO_2 undergoes electron-impact dissociation to produce CO and O radicals. Steam also dissociates to form H radicals and additional O radicals. These radicals dominate the subsequent reaction pathways. The O radicals actively attack hydrocarbon fragments, including PAHs and aliphatic species, leading to their oxidation into CO and H_2 [60]. The continuous consumption of intermediates suppresses the growth of aromatic structures. In parallel, reforming reactions contribute significantly to syngas formation. CH_4 reacts with steam through steam methane reforming (SMR) to produce H_2 and CO. Dry reforming between hydrocarbons and CO_2 also generates CO and H_2. The water-gas shift (WGS) reaction further enhances hydrogen

production by converting CO and H_2O into CO_2 and H_2. These coupled reactions increase the overall H_2 yield in the system. Furthermore, fragmentation and charring of heavier intermediates lead to the formation of solid carbon and smaller gaseous species. The solid carbon reacts with CO_2 via the Boudouard reaction to produce additional CO. Although recombination between CO and O radicals to form CO_2 can occur, this pathway is kinetically limited at elevated plasma temperatures. The rapid consumption of O radicals in oxidation and reforming reactions further suppresses recombination. Overall, the combined effects of electron-driven dissociation, radical-mediated oxidation, and reforming reactions enhance the conversion of LDPE into hydrogen-rich syngas. The process favors the production of H_2 and CO while minimizing the persistence of intermediate hydrocarbons and solid residues.

3.7 Comparison study of developed models for operational and environmental performance

In order to analyze the findings of this research, a comprehensive comparative analysis was conducted across the optimal operating points established in both the physical experiments and the ASPEN PLUS thermodynamic simulations. The comparison evaluates the four primary gasification scenarios investigated to produce optimum syngas, reported in volume percentage, as follows:

1) Experimental (CO_2 plasma gasification): Utilizing 1.5 kg/h CO_2 as gasification agent in the Ar-CO_2 thermal arc plasma chamber.
2) Model I (CO_2 plasma gasification): Utilizing 1.5 kg/h CO_2 as gasification agent
3) Model II (steam plasma gasification): utilizing 1.0 kg/h steam as gasification agent
4) Model III (steam-CO_2 plasma gasification): utilizing 0.75 kg/h steam and 0.25 kg/h CO_2.

3.7.1 Operational performance

To assess the volumetric productivity of the plasma gasification system, the SSY was calculated for all simulated models and the experiment performed. The evolution of the Specific Syngas Yield for pure CO_2 and pure steam theoretical models, plotted alongside the physical experimental benchmark, is illustrated in Figure 11 (a). The graphical trends reveal two distinct kinetic phases dictating gas production. The first phase, the "carbon conversion zone," is characterized by a steep, linear increase in SSY. As the pure gasification agents are incrementally injected, they actively volatilize the solid LDPE carbon into gaseous molecules via the boudouard and reforming reactions. Because solid carbon has negligible volume, converting it into permanent gas (CO, CH_4, H_2) results in higher volumetric expansion. Model

II (Steam) fundamentally outpaces Model I (CO_2) in specific yield. At the stoichiometric optimum for CO_2 gasification (1.5 kg/h), the model produces an SSY of 3.55 Nm^3/kg. The similar yield (3.4 Nm^3/kg) is reported by Sikarwar et al. [27] for RDF processing and Tamošiūnas et al. [31] whose carbon and volatile percentage were similar to the LDPE sample used in this study. However, the stoichiometric optimum for steam gasification (1.0 kg/h) yields a significantly larger volume of 4.48 Nm^3/kg. This disparity is rooted in reaction stoichiometry: the boudouard reaction ($C + CO_2 \rightleftharpoons 2CO$) produces two moles of gas per mole of converted carbon. Whereas the water-gas and steam methane reforming reactions heavily liberate the hydrogen trapped within the polymer, physically multiplying the total moles of gas generated. Once the respective agents reach their optimal carbon conversion thresholds (around complete conversion), the system enters the second phase: "over-oxidation." Here, adding excess steam or CO_2 does not extract any additional carbon from the plastic. The SSY continues to rise, but at a visibly reduced slope, as the increase in total volume is driven solely by the physical accumulation of unreacted, injected gas molecules acting as thermal diluents. The experiment conducted (1.5 kg/h CO_2) produced an SSY of 2.90 Nm^3/kg.

To understand the volumetric impact of simultaneous dual-agent injection, the SSY for Model III is mapped as a 3D surface plot in Figure 11 (b). The 3D-surface plot visually captures the intersection of the two unique volume-generating pathways. The SSY rises sharply from the under-oxidized baseline as both steam and CO_2 actively convert solid carbon into gas; so, the SSY surface continues to ascend. Once the carbon is fully cracked, the resulting plateau transitions into an upward-sloping plane where excess injected gas artificially inflates the product volume. The optimal "hydrogen-optimized condition" point utilizing 0.75 kg/h of steam alongside 0.25 kg/h of CO_2 is positioned precisely at the critical "crease" of the surface. At this point, the SSY is established at an impressive 4.30 Nm^3/kg. This finding theoretically validates the mixed-agent strategy: it captures nearly the entire massive volumetric benefit of steam reforming (4.48 Nm^3/kg) while simultaneously utilizing the CO_2 to stabilize the chemistry, firmly securing the operating point before entering the over-oxidized, diluent-heavy slopes of the 3D plane.

The syngas composition for the given optimum condition is compared in Figure 11 (c). As illustrated, transitioning from CO_2 to steam-based gasification fundamentally alters the thermochemical breakdown of the LDPE waste. At a matched feed rate of 1.5 kg/h CO_2, both the experimental and modelled CO_2 gasification runs yielded a CO-dominant syngas (63.0 vol% and 67.7 vol% CO, respectively) driven by the aggressive boudouard reforming reaction.

Conversely, replacing the CO_2 entirely with 1.0 kg/h of steam flipped the dominant product strictly to hydrogen (57.1 vol% H_2) via steam methane reforming and the water-gas reaction. However, the mixed-agent model (0.75 kg/h steam + 0.25 kg/h CO_2) provided the most balanced and synergistic composition. By utilizing a hybrid gasification approach, the H_2 yield was maintained at an exceptionally high level (52.0 vol%), while the CO yield was stabilized at 43.6 vol%. This operating condition successfully suppressed the formation of inert CO_2 (restricted to just 1.18 vol%), yielding a combined combustible gas purity (> 95.6 vol%) that matches or exceeds the pure agent approaches without their respective operational downsides.

The energetic performance of each configuration is compared in Figure 11 (d), revealing critical insights into the real-world efficiency of the plasma system relative to its thermodynamic limits. LHV, and CGE were calculated for each scenario. The LHV (MJ/Nm^3) of the product gas was determined based on the combustible volume fractions (Y_{H_2}, Y_{CO}, Y_{CH_4}) using Equation 3. Correspondingly, the CGE was calculated using Equation 4, factoring in the LDPE mass feed rate (1 kg/h) and the corrected empirical LHV of the LDPE feedstock (38.10 MJ/kg), and the respective electrical power inputs for the experimental and simulation (32.4 MJ/h; 9 kW). The LHV remained highly competitive across all methods, ranging from 11.8−14.5MJ/Nm^3. The CO_2 models exhibited the highest volumetric LHV (13.7−14.5 MJ/Nm^3) due to the higher calorific density of carbon monoxide compared to hydrogen, coupled with the high retention of residual methane (10.0 %). The steam-based models exhibited slightly lower volumetric LHVs (11.8−12.3 MJ/Nm^3) as the heavy carbon molecules were aggressively cracked into lighter, less dense hydrogen gas. The LHV of the syngas produced in the current study surpasses the values reported for the CO_2 plasma gasification of bakelite [61] and RDF [27], while remaining highly comparable to pure CO_2-RDF gasification results [21]. However, it is slightly lower than the exceptionally high calorific value of 16.46 MJ/Nm^3 achieved during the pure CO_2 DC arc plasma gasification (2 kW) of computer keyboard plastics [59]. The reason of higher LHV might be higher CO vol% (52 vol%) in comparison to H_2 (32 vol%) with a very high-power input of 2 kW for 40 g/10 min acrylonitrile butadiene styrene (ABS) plastic waste processing.

At the power input of 9 kW (32.4 MJ/h), the CGE reflect strictly the chemical conversion efficiencies of each process. The experimental run achieved a highly robust CGE of 69.0 %. The baseline CO_2 thermodynamic model returned a CGE of 73.1 %; this 4.1 % discrepancy accurately quantifies the energy lost to the kinetic limitations and thermal gradients within the plasma chamber. The steam-based simulations demonstrated that maximizing the hydrogen

yield corresponds to maximizing the total energetic yield. The steam and mixed-agent models achieved nearly identical, CGEs of 74.9 % and 74.8 %, respectively. This conclusively demonstrates that the mixed gasification approach (0.75 kg/h steam and 0.25 kg/h CO_2) is the ultimate optimal configuration. The CGE of the current study is higher than the several reported studies such as CO_2 plasma gasification of RDF [21,27], ABS plastic [59], medical plastic waste [31] etc. The similar trend (51.7 %) found with steam plasma gasification of surgical mass [32].

To further establish the robustness and industrial viability of the plasma gasification processes evaluated in this study, the CCE was analyzed across the full sensitivity ranges of the theoretical models and compared directly against the physical experiment. For the experiment conducted at a feed rate of 1.5 kg/h CO_2, the measured syngas yield is 2.90 Nm^3/h. The continuous CCE trends for the single-agent theoretical simulations (Model I and II), alongside the experimental benchmark, are mapped in the 2D plot in Figure 11 (e). The ASPEN PLUS thermodynamic models, which operate on the principle of Gibbs free energy minimization, demonstrate a distinctly linear CCE progression during the "under-oxidation" phase. Without any gasification agent flow, the system relies entirely on the minimal oxygen provided by the carrier gas (plasma forming gas: CO_2 and Ar), yielding a baseline CCE of roughly 70.4 % due to higher char formation. As pure CO_2 (Model I) is incrementally introduced, the CCE scales proportionately via the boudouard reaction until it reaches a thermodynamic threshold of 100 % at the stoichiometric optimum of 1.5 kg/h. Similar CCE is reported by Sikarwar et al for the CO_2 plasma gasification of RDF waste processing [27]. Model II demonstrates that pure steam is an even more aggressive carbon-cracking agent per unit mass; driven by the heterogeneous water-gas reaction, the steam model hits the 100 % conversion plateau much earlier, at a flow rate of just 1.0 kg/h. Beyond these mass-flow, adding excess agent merely dilutes the syngas and triggers the water-gas shift reaction, providing no further benefit to carbon conversion. Whereas the experiment conducted at 1.5 kg/h CO_2 results in 91.4 % CCE calculated using Equation 5. It diverges slightly from the models, capturing the real-world artifacts of thermal plasma kinetics. The extremely rapid transit of the feedstock through the thermal gradient zones of the plasma chamber restricts the residence time, preventing the endothermic reforming reactions from reaching absolute completion. Nevertheless, the experimental run proves the intense degradation capability of the Ar-CO_2 thermal arc plasma, successfully mobilizing the vast majority of the polymer's dense carbon chain into the gas phase.

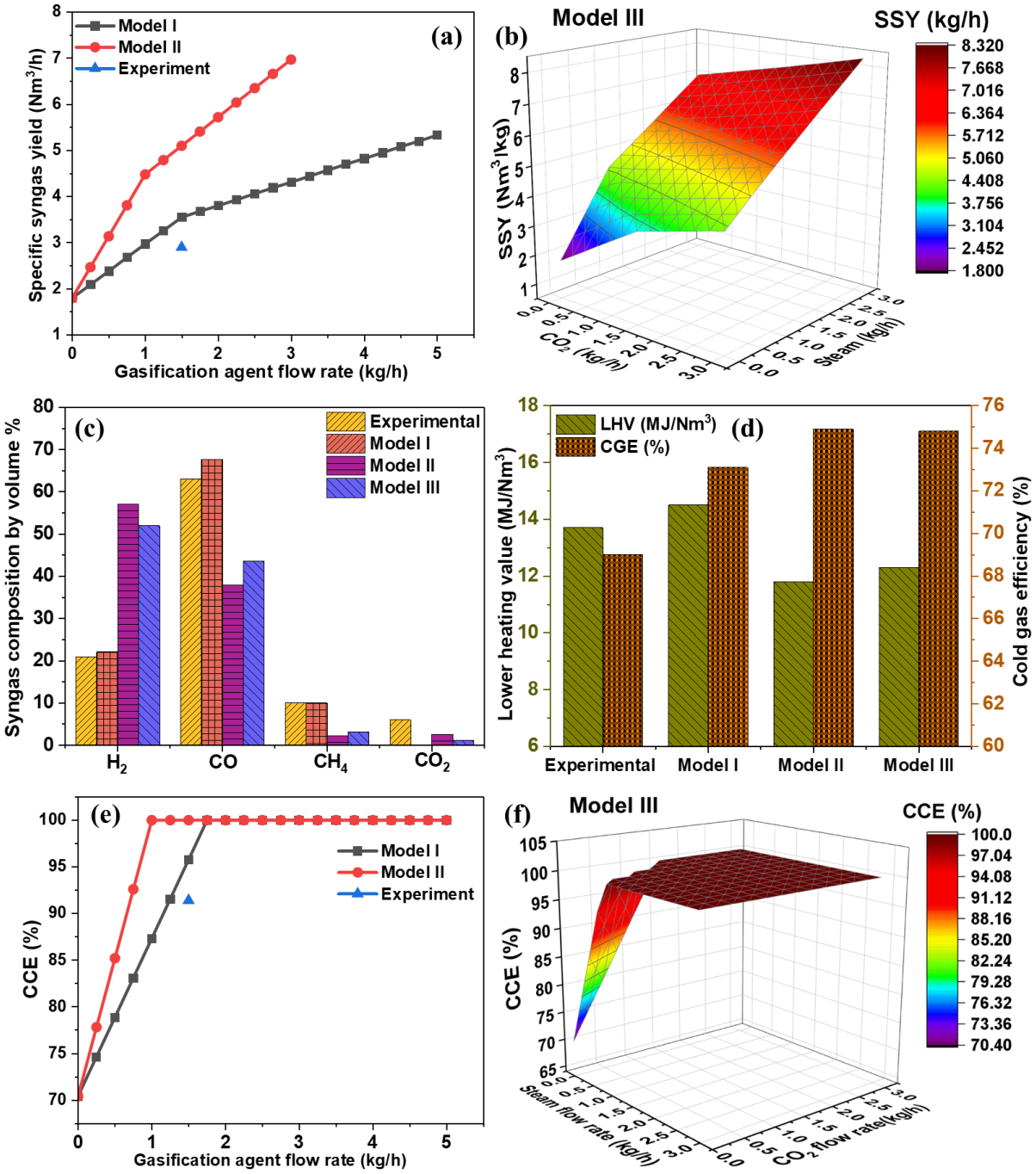

Figure 11. Comparison study of (a) SSY production from model I & II, simulated and experiment conducted, (a) SSY production from for mixed gasification agent (model III), (c) optimal syngas compositions across experimental and models studies, (d) LHV and CGE across optimal conditions for experimental and models, (e) CCE (%) for model I & II, simulated and experiment conducted, and (f) CCE (%) for mixed gasification agent (model III).

The mixed gasification agent approach involves the simultaneous variation of two distinct gases; the resulting CCE is mapped as a 3D surface plot in Figure 11 (f). This visualization captures the highly synergistic effect that steam and CO_2 exert on the carbon conversion. Initial

result in absence of gasification agents was similar to the experiment and Models (I & II), producing majority of char and CH_4 as the primary product. However, while both agents are co-fed into the system, steam rapidly consumes solid carbon via the water-gas reaction whereas CO_2 concurrently drives the Boudouard reaction. This dual reaction rapidly increases the CCE (visualized through a steep contour slope in Figure 11 (f)) toward the thermodynamic threshold (complete conversion). The defining advantage of the mixed-agent approach is visually evident on the 100% surface plateau. By blending the agents, the system achieves total carbon volatilization at substantially lower individual flow rates than utilizing either agent in isolation. The identified "hydrogen-optimized condition" point utilizing just 0.75 kg/h of steam alongside a minimal 0.25 kg/h of CO_2 meets precisely on the leading edge of this complete conversion plateau. This 3D analysis confirms that the mixed gasification approach not only maximizes hydrogen yield and syngas purity but theoretically delivers the absolute highest possible utilization of the raw plastic feedstock without pushing the system into thermal dilution.

To consolidate the operational findings and facilitate a clear comparison across the evaluated gasification scenarios, a comprehensive performance summary is presented in Table 3. This table outlines the specific gasification agent flow rates, resulting syngas compositions, and all operational performance parameters studied. While maximizing these operational metrics and energy recovery is fundamental for process viability, assessing the primary environmental impact is equally critical is discussed in the subsequent sections.

Table 3. Summary of optimal operational parameters for experimental and modelled gasification process.

Parameters	Experimental	Model I	Model II	Model III
Gasification Agent	CO_2	CO_2	Steam	Mixed (Steam + CO_2)
Agent Flow Rate (kg/h)	1.50	1.50 (optimum)	1.00 (optimum)	0.75 (Steam) + 0.25 (CO_2) (optimum)
Syngas Composition (vol. %)				
H_2	21.00	22.18	57.14	51.96
CO	63.00	67.72	37.93	43.65
CH_4	10.00	10.01	2.31	3.21
CO_2	6.00	0.16	2.61	1.18
Specific Syngas Yield (Nm^3/kg)	2.90	3.55	4.48	4.30
Lower Heating Value (MJ/Nm^3)	13.8	14.5	11.8	12.3
Cold Gas Efficiency (%)	69.0	73.1	74.9	74.8
Carbon Conversion Efficiency (%)	91.4	100.0	100.0	100.0

3.7.2 Environmental performance

To evaluate the environmental impact of the proposed plasma gasification systems, a comprehensive carbon footprint assessment was conducted. The specific mass of CO_2 released into the atmosphere per kilogram of LDPE waste processed by the plasma models was calculated and directly benchmarked against established plastic waste management paradigms: incineration and conventional gasification. Providing a highly conservative and realistic environmental assessment, the CO_2 emissions for the plasma models were derived incorporating real-world kinetic limitations. For Model I (1.5 kg/h CO_2), the physical experimental data was utilized directly, resulting in exactly 0.34 kg of CO_2 released per kilogram of plastic processing. For Model II (steam) and Model III (mixed agent), the thermodynamic CO_2 volume fractions were extrapolated by adding the approximately 6.0 % kinetic error margin observed in the experiment. This resulted in realistic extrapolated footprints of 0.53 kg and 0.61 kg of CO_2/kg waste for Model II and Model III respectively. The resulting environmental performance comparison is illustrated in Figure 12 (a). The comparison analysis incineration and gasification with plasm a gasification models are as follows:

- Incineration: Conventional waste-to-energy incineration relies on total exothermic oxidation to generate heat. It generates around 2.90 kgCO_2/kg plastic waste processing [62]. Given the exceptionally dense carbon fraction of the LDPE feedstock (85.9 %), incineration acts as a massive carbon emitter. Whereas all three plasma models achieve 79 % to 88 % reduction in greenhouse gas emissions compared to incineration by mobilizing the carbon into combustible syngas rather than fully oxidizing it.
- Gasification: Conventional gasification systems (air gasification) exhibit the lowest initial direct emissions of around an average of 0.25 kgCO_2/kg plastic [62]. However, this technology relies on partial combustion, which produces high volumes of complex tars and low-quality syngas (with inferior hydrogen yields) that require extensive downstream energy to purify. Model I exhibits comparative CO_2 (0.35 kg vs 0.25 kg) footprint while others proposed plasma models (Models II and III) predict slightly higher direct emissions (0.53 kg and 0.61 kg), due to use of steam and mixed gasification agent respectively. Using steam as a gasification agent improves hydrogen concentration at the expense of additional CO_2 generation from water gas shift reaction. Overall additional CO_2 is compensated for producing exceptionally pure, tar-free syngas with massive hydrogen yields (> 50 vol%).

3.8 Carbon capture and utilization (CCU) for net-zero process carbon footprint

While the comprehensive carbon footprint of the thermal arc plasma gasification models (0.34 to 0.61 kg CO_2/kg LDPE) represents a profound environmental improvement over conventional waste-to-energy pathways, the ultimate objective of this process is to establish a truly circular, net-zero carbon waste management solution. To achieve this, the generated syngas must be integrated with downstream gas purification technology, specifically Pressure Swing Adsorption (PSA). By incorporating a PSA model unit that routinely operates at a CO_2 separation efficiency of 90 % or higher the trace CO_2 generated during the plasma gasification process can be actively recovered. Crucially, because the proposed thermal arc plasma models fundamentally require CO_2 to operate (as a carrier gas to sustain the Ar-CO_2 arc and as a chemical gasification agent to drive the Boudouard reaction), the recovered CO_2 does not need to be sequestered; it can be directly recirculated back into the plasma-forming carrier gas feed line.

By closing this carbon loop, the facility offsets its own operational requirements, actively suppressing the net carbon footprint of processing the LDPE waste to near-zero (excluding grid electricity demands). To quantify the efficiency of this CCU integration model, a detailed mass balance was conducted across the three operational models, comparing the total CO_2 fed into the chamber against the total CO_2 generated in the syngas and the fraction of CO_2 successfully recovered by the PSA unit (assuming a conservative 90 % recovery efficiency). The results are illustrated in Figure 12 (b). The proposed recirculation model for plasma gasification technology targeting net zero carbon processing is shown in Figure 12 (c).

- Model I: The CO_2 gasification model relies heavily on external carbon input, demanding a total feed of 2.04 kg/h (0.54 kg/h carrier gas and 1.50 kg/h active agent). As established previously, the real-world kinetics of the physical plasma chamber resulted in a trace generation of 0.34 kg/h of CO_2 in the product syngas. Passing this exhaust through the PSA unit recovers 0.31 kg/h of CO_2. When this 0.31 kg is recirculated, the net CO_2 emission drops to a negligible 0.03 kg/h.
- Model II: In the steam gasification model, CO_2 is solely utilized as the carrier gas (0.54 kg/h), while 1.0 kg/h of steam serves as the gasification agent. The extrapolated thermodynamic simulation generated 0.53 kg/h of CO_2. The downstream PSA unit captures 0.48 kg/h of this exhaust. Recirculating this captured CO_2 fulfils nearly 89 % of the 0.54 kg/h carrier gas requirement. Consequently, the net CO_2 emission to the atmosphere is reduced to just 0.05 kg/h.

- Model III : The hydrogen-optimized mixed-agent approach requires a total CO_2 feed of 0.79 kg/h (0.54 kg/h carrier gas & 0.25 kg/h co-fed agent) alongside 0.75 kg/h of steam. The extrapolated trace generation of CO_2 in the syngas was calculated at 0.61 kg/h. After processing through the 90 % efficient PSA unit, exactly 0.55 kg/h of high-purity CO_2 is recovered. By recirculating this 0.55 kg/h back into the plasma forming carrier gas feed line, the facility covers almost 70% of its total operational carbon requirement. The net physical emission released to the atmosphere from the uncaptured exhaust drops to a highly manageable 0.06 kg/h per kilogram of plastic processed.

The mass balance proves that regardless of the specific agent ratio utilized, the graphite electrode-based thermal arc plasma gasification of LDPE operates at a permanent carbon deficit. Because the endothermic reforming and Boudouard reactions convert the recirculated CO_2 molecules, converting them into permanent, high-energy CO and H_2, the generated syngas CO_2 is never enough to sustain the operation independently. By capturing and utilizing the exhaust, the process effectively achieves a net-zero carbon footprint regarding the degradation of the plastic waste itself, securing its status as a highly sustainable, carbon-negative pathway for clean hydrogen production.

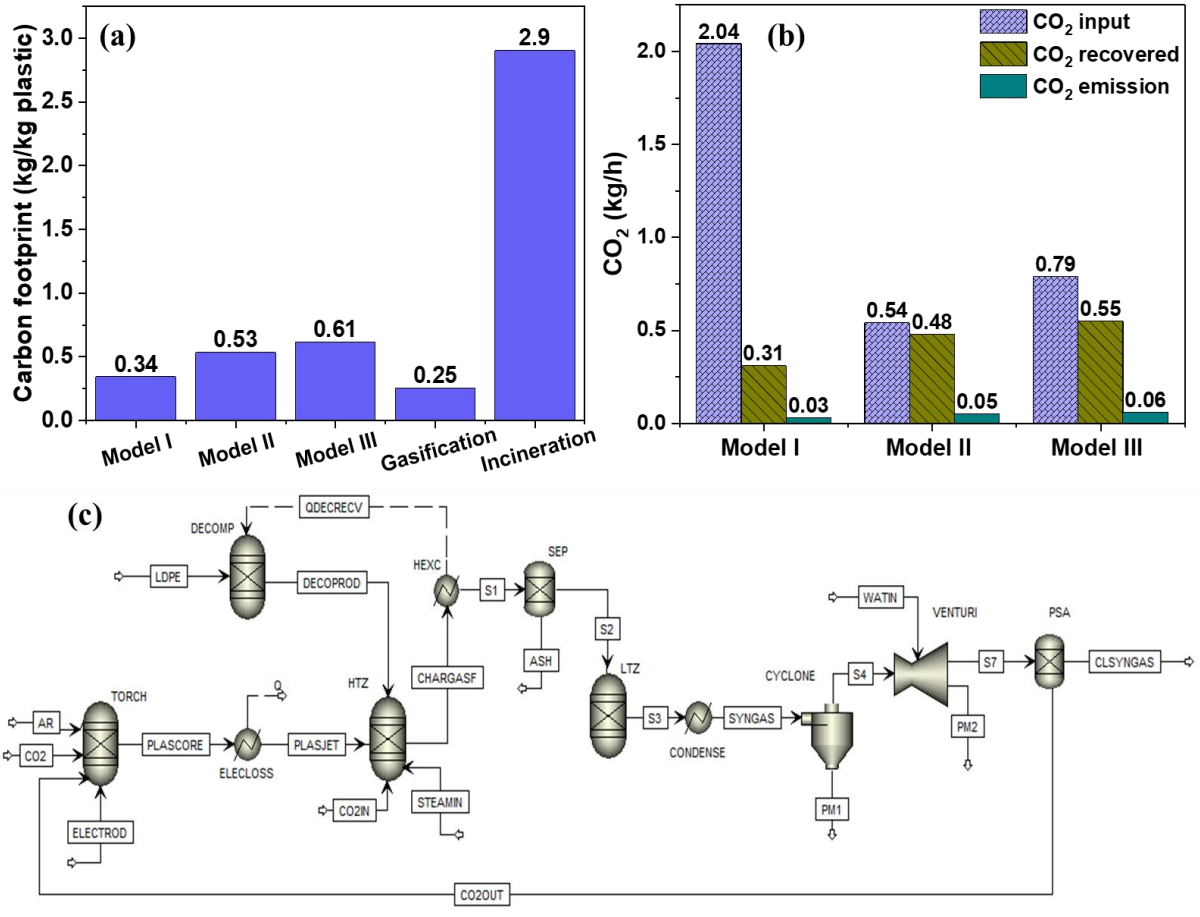

Figure 12. (a) Carbon footprint comparison of plasma gasification models vs. direct output from waste-to-energy technologies, (b) prediction of final CO_2 emission from CCU model integration utilizing a PSA unit to recover and recirculate generated CO_2 for making a net zero carbon plasma gasification technology, and (c) ASPEN PLUS model for recirculation of CO_2 for proposing a net zero carbon plasma gasification technology.

3.9 Preliminary study for commercialization of technology for upcoming hydrogen economy

Looking to the upcoming hydrogen economy, the proposed plasma gasification system was investigated in terms of H_2 production capability and its associated energy competitiveness. Considering this aspect as a core objective, H_2 yield and the SEC for hydrogen generation serve as the ultimate determining metrics. The comparative results for H_2 yield and SEC across the four optimal operating conditions are presented in Figure 13 (a). When utilizing CO_2 as the sole gasification agent, the system is fundamentally starved of hydrogen production. The experiment conducted and theoretical Model I (1.5 kg/h CO_2) achieved H_2 yields of just 0.61 Nm^3/kg and 0.78 Nm^3/kg, respectively, as all hydrogen was forced to originate solely from the decomposition of the polymer's internal C-H bonds. Because the plasma arc continuously drew 9.0 kW of power to produce this limited volume, the resulting SEC values were exceptionally high, registering at 14.75 kWh/Nm^3 for the experiment and 11.54 kWh/Nm^3 for the simulated model. These high values indicate that pure CO_2 plasma gasification, while excellent for synthesizing carbon monoxide, is economically unviable if the primary industrial target is H_2 production. The introduction of steam to the plasma environment radically alters the economic viability of the process.

The steam plasma gasification simulation (Model II at 1.0 kg/h) demonstrated the thermodynamic maximum of the system, driving the H_2 yield of 2.56 Nm^3/kg. Correspondingly, the energy demand dropped, yielding an optimal SEC of just 3.52 kWh/Nm^3H_2. However, as established previously, pure steam systems face severe physical handling and phase-change complexities that hinder stable operations. The mixed-agent approach (Model III) successfully bridges the gap. By utilizing the " H_2-optimized condition" (0.75 kg/h steam and 0.25 kg/h CO_2), the system retains a massive H_2 yield of 2.23 Nm^3/kg while maintaining an extremely competitive SEC of 4.04 kWh/Nm^3 H_2. It confirms the principal hypothesis of the study: a mixed steam CO_2 gasification agent perfectly leverages the immense hydrogen-liberating power of steam reforming while relying on the CO_2 co-feed to stabilize the gas mixture and lower the physical water-handling burden. The SEC of 4.04

kWh/Nm^3 is highly competitive with modern commercial water electrolysis technologies (which typically range from 4.5 to 5.5 kWh/Nm^3).

While the lab-scale investigations robustly validate the chemical pathways and optimal agent ratios required to maximize hydrogen yield from LDPE waste, the absolute values of the SEC observed at this scale (4.04 to 14.75 kWh/Nm^3 H_2) remain somewhat elevated compared to conventional industrial technologies. This high SEC is a well-documented limitation inherent to lab-scale thermal arc plasma reactors. In small-volume chambers processing minimal feed rates (1.0 kg/h), the plasma torch must continuously draw a baseline electrical load (9.0 kW) simply to sustain the ionization of the Ar-CO_2 carrier gas and overcome the disproportionately high heat losses caused by the reactor's large surface area-to-volume ratio. Consequently, the energy penalty is artificially inflated when normalized against the small volume of syngas produced.

However, the energy dynamics of graphite electrode-based thermal arc plasma gasification do not scale linearly with the mass feed rate. As demonstrated in recent pilot-scale applications such as the 50 kg/h MSW plasma chamber utilized by Rana et al., the required power input flattens significantly as the system scales up [20]. A pilot-scale reactor processing 10 kg/h of concentrated plastic waste requires an operating power of approximately 30 kW to maintain the required high-temperature gradient zone, representing merely 3.3 times increase in electrical load for 10 times increase in feedstock throughput. Similar power input (28−48 kW excluding 30% cooling loss of plasma torch) of plasma gasification technology was reported by Tamošiūnas et al., for 10 kg of medical plastic waste processing [31]. This non-linear relationship occurs because larger continuous-feed reactors benefit from superior internal thermal retention, steady-state autothermal contributions from the syngas, and a drastically reduced baseline ionization demand per unit of mass.

To evaluate the true industrial potential of the proposed models, a pilot-scale thermodynamic extrapolation was conducted. Assuming identical stoichiometric conversion efficiencies and gasification agent ratios established at the lab scale, the models were scaled to a 10 kg/h LDPE feed rate operating under a steady 30 kW plasma power input. As illustrated in Figure 13 (b), the transition from lab-scale to pilot-scale yields a dramatic, uniform reduction in the SEC across all operational modes. For Model I (pure CO_2), scaling the process drops the SEC drops from 11.54 kWh/Nm^3 H_2 to 3.85 kWh/Nm^3 H_2. While this is a significant improvement, pure CO_2 gasification remains comparatively energy-intensive due to the inherently low volume of hydrogen produced (7.8 Nm^3/h) solely from plastic waste. Whereas

the hydrogen-optimized models demonstrate energetic efficiencies at the pilot scale. Model II (steam) generates 25.6 Nm^3/h of hydrogen, plunging the SEC to just 1.17 kWh/Nm^3 H_2. Most importantly, Model III, the optimal mixed-agent approach utilizing 7.5 kg/h steam and 2.5 kg/h CO_2 generates 22.3 Nm^3/h of H_2 at an SEC of exactly 1.35 kWh/Nm^3 H_2.

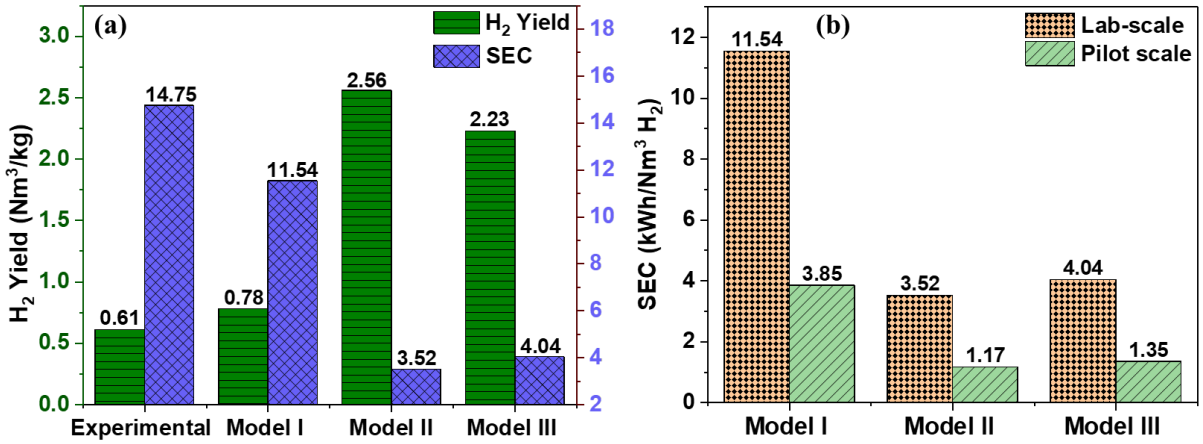

Figure 13. (a) Comparison of absolute H_2 Yield and SEC across the four optimal experimental and modelled conditions, and (b) Comparison of SEC between the lab scale and pilot-scale operations.

The projected SEC of 1.35 kWh/Nm^3 H_2 for the mixed-agent system firmly establishes the commercial viability of the technology. It significantly undercuts the energy demands of modern commercial water electrolysis which typically requires 4.5 to 5.5 kWh/Nm^3 H_2 [63]. It proves that plasma-assisted waste gasification is not merely a waste management strategy, but a highly competitive method for hydrogen production. Ultimately, this comparison serves as a critical preliminary study for industrial scale-up. The 1.0 kg/h lab-scale data successfully solved the chemical challenge, proving that mixing steam and CO_2 prevents the physical handling issues of pure steam while maximizing carbon conversion efficiency (> 91.4 %) and suppressing CO_2 dilution in the syngas. Concurrently, the 10 kg/h pilot-scale projection resolves the economic challenge, confirming that graphite electrode thermal arc plasma can process dense polyolefin wastes into high-purity hydrogen at an energy cost well below the threshold of conventional green hydrogen production technologies.

4 Conclusion

This study successfully demonstrated the thermochemical and environmental viability of graphite electrode-based DC thermal arc plasma gasification for LDPE waste valorization. The novel ASPEN PLUS thermodynamic model was developed to overcome the limitations of conventional simulations by explicitly incorporating carrier gas dissociation, thermal

quenching, and electrode sublimation. The model was successfully validated against physical experiments utilizing 1.5 kg/h CO_2, demonstrating strong predictive alignment for syngas composition (21.0 vol% H_2, 63.0 vol% CO, 10.0 vol% CH_4) and accurately capturing the kinetic limitations inherent to physical plasma reactors.

The investigation into different gasifying mediums highlighted the distinct advantages of a hybrid system over single-agent operations. While utilizing CO_2 as gasification agent (model I) favored CO generation, and steam (model II) drove hydrogen production at the cost of thermal dilution, mixed agents (model III) effectively resolved these inherent chemical trade-offs. By co-feeding 0.75 kg/h of steam with 0.25 kg/h of CO_2, the system established a highly synergistic environment that maximized the specific syngas volume (4.30 Nm^3/kg) and predicted complete carbon conversion. This optimum balance successfully restricted the unwanted water-gas shift reaction, keeping CO_2 formation around 1.18 vol% and resulting in premium-grade syngas with over 95 vol% combustible species. Consequently, the mixed-agent process achieved a remarkable CGE of 74.8 %, proving that strategically mixing the agents fundamentally optimizes energy recovery.

From an environmental perspective, the plasma models exhibited a 79 % to 88 % reduction in direct CO_2 emissions compared to conventional incineration. By integrating the CCU model with a 90 % efficient PSA unit, the unreacted CO_2 exhaust can be captured and recirculated directly into the carrier gas feed line. This closed-loop system reduces the net carbon footprint of the mixed-agent process to an insignificant amount of 0.06 kg CO_2 per kg of plastic waste processed, effectively transforming the waste treatment facility into an active carbon sink.

Finally, the study establishes technology's commercial readiness for the upcoming hydrogen economy. While the lab-scale mixed-agent system recorded a SEC of 4.04 kWh/Nm^3 H_2, pilot-scale extrapolations (10 kg/h feed, 30 kW DC power input) demonstrated a dramatic reduction in energy demand to just 1.35 kWh/Nm^3 H_2. This significantly undercuts modern commercial water electrolysis energy demands (4.5 to 5.5 kWh/Nm^3 H_2), proving that graphite electrode-based Ar-CO_2 plasma gasification is a highly competitive, carbon-negative pathway for clean hydrogen synthesis.

Credit authorship contribution statement

Tejashwi Rana: Conceptualization, Methodology, Formal analysis, Investigation, Validation, Software, Writing – original draft. **Aishik Basu Mallick:** Methodology, Formal analysis, Validation. **Kaushik Kundu:** Software, Formal analysis, Investigation. **Kamal K. Pant:**

Supervision, Resources. **Satyananda Kar:** Conceptualization, Methodology, Supervision, Validation, Writing – review & editing.

Declaration of competing interests

The authors certify that there is no conflict of interest with any financial organization regarding the material discussed in the manuscript.

Acknowledgment

The authors acknowledge Invest India and Principal Scientific Advisor (PSA) to the Government of India (GoI) for financial assistance in conducting the research under the Waste to Wealth mission. The authors acknowledge Department of Chemical Engineering, Indian Institute of Technology Delhi for giving permission to use software ASPEN PLUS V14.0 for academic purposes. The authors also acknowledge Mr. Suryasunil Rath and Mr. Pratyay Chattopadhyay from Department of Energy Science and Engineering, Indian Institute of Technology Delhi for helping in optical emission spectrometer (OES) analysis.

Data availability

Data will be made available on request.

References

[1] Kibria MG, Masuk NI, Safayet R, Nguyen HQ, Mourshed M. Plastic Waste: Challenges and Opportunities to Mitigate Pollution and Effective Management. Int J Environ Res 2023;17:20. https://doi.org/10.1007/s41742-023-00507-z.

[2] Geyer R, Jambeck JR, Law KL. Production, use, and fate of all plastics ever made. Sci Adv 2017;3:e1700782. https://doi.org/10.1126/sciadv.1700782.

[3] Ellen MacArthur Foundation and World Economic Forum. The New Plastics Economy: Rethinking the future of plastics. Ellen MacArthur Found 2016:120.

[4] Balaji AB, Liu X. Plastics in Circular Economy: A Sustainable Progression. In: Liu L, Ramakrishna S, editors. An Introd. to Circ. Econ., Singapore: Springer Singapore; 2021, p. 159–78. https://doi.org/10.1007/978-981-15-8510-4_9.

[5] Ayuso-Díaz I, Perez-Gil S, Lopez G, Santamaria L, Antoñanzas-González FJ. Progress on waste plastics gasification process: A review of operating conditions, reactors and catalysts for clean syngas production and tar abatement. Int J Hydrogen Energy 2025;148:150000. https://doi.org/10.1016/j.ijhydene.2025.06.190.

[6] Ghosh SK, Chakraborty SS, Rana T, Karstensen KH, Saha PK. Legislative Support to Curb Marine Littering through Wastes Co-processing by Promoting Circular Economy. Eff Waste Manag Circ Econ 2022:27–41. https://doi.org/10.1201/9781003231608-4.

[7] Khairul Anuar SZ, Nordin AH, Nur Husna SM, Yusoff AH, Paiman SH, Md Noor SF, et al. Recent advances in recycling and upcycling of hazardous plastic waste: A review. J Environ Manage 2025;380:124867. https://doi.org/10.1016/j.jenvman.2025.124867.

[8] Obuzor GU, Onyedikachi UB. Chemical Leaching into Food and the Environment Poses Health Hazards. In: Nwaichi EO, editor. Mod. Heal. Dis. Diagnosis Acc. from STEM Women, Cham: Springer Nature Switzerland; 2023, p. 129–48. https://doi.org/10.1007/978-3-031-34963-8_14.

[9] Sanjaya E, Abbas A. Plasma gasification as an alternative energy-from-waste (EFW) technology for the circular economy: An environmental review. Resour Conserv Recycl 2023;189:106730. https://doi.org/10.1016/j.resconrec.2022.106730.

[10] Dossow M, Bastek S, Spliethoff H, Fendt S. Electrifying biomass-to-liquid processes using plasma-assisted entrained flow gasification. Energy Convers Manag 2025;341:120049. https://doi.org/10.1016/j.enconman.2025.120049.

[11] Zhao B, Hu X, Lu J. Analysis and discussion on formation and control of dioxins generated from municipal solid waste incineration process. J Air \& Waste Manag Assoc 2022;72:1063–82. https://doi.org/10.1080/10962247.2022.2100843.

[12] Rida Galaly A, Van Oost G, Dawood N. Sustainable Plasma Gasification Treatment of Plastic Waste: Evaluating Environmental, Economic, and Strategic Dimensions. ACS Omega 2024;9:21174–86. https://doi.org/10.1021/acsomega.4c01084.

[13] Mallick AB, Prakash GV, Kar S, Narayanan R. Development of a pulse modulated sub-radio frequency power supply for atmospheric pressure plasma devices. Rev Sci Instrum 2023;94. https://doi.org/10.1063/5.0173873.

[14] Fathi J, Mašláni A, Hlína M, Lukáč F, Mušálek R, Jankovský O, et al. Multiple benefits of polypropylene plasma gasification to consolidate plastic treatment, CO2 utilization, and renewable electricity storage. Fuel 2024;368:131692. https://doi.org/10.1016/j.fuel.2024.131692.

[15] T P R, Kar S. Glow-to-arc discharge transitions in a radio frequency atmospheric pressure plasma jet. Phys Fluids 2024;36. https://doi.org/10.1063/5.0218872.

[16] Rath S, Kar S. Microwave atmospheric pressure plasma jet: A review. Contrib to Plasma Phys 2025;65(2):e202400036. https://doi.org/10.1002/ctpp.202400036.

[17] Rath S, Das P, Pandey P, Kar S. Uncertainty-Aware Machine Learning-Based Prediction of Plasma Parameters in a Microwave Atmospheric Pressure Plasma Jet. Phys Chem Chem Phys 2026;28. https://doi.org/10.1039/D5CP04364F.

[18] Demir F, Yurtkuran E, Unal R, Ozsunar AK. 3D Cfd Modelling of Non-transferred Argon Plasma Torch. Mater Today Proc 2020;32:12–7. https://doi.org/10.1016/j.matpr.2020.05.510.

[19] Rana T, Kar S. Study of preheating temperature and electrode consumption in a plasma gasification system for waste processing. J Energy Inst 2025;120:102122. https://doi.org/10.1016/j.joei.2025.102122.

[20] Rana T, Kar S. Assessment of energy consumption and environmental safety measures in a plasma pyrolysis plant for eco-friendly waste treatment. J Energy Inst 2024;114:101617. https://doi.org/10.1016/j.joei.2024.101617.

[21] Mallick R, Vairakannu P. Experimental studies on CO2-thermal plasma gasification of refused derived fuel feedstock for clean syngas production. Energy 2024;288:129766. https://doi.org/10.1016/j.energy.2023.129766.

[22] Sikarwar VS, Peela NR, Vuppaladadiyam AK, Ferreira NL, Mašláni A, Tomar R, et al. Thermal plasma gasification of organic waste stream coupled with CO(2)-sorption enhanced reforming employing different sorbents for enhanced hydrogen production. RSC Adv 2022;12:6122–32. https://doi.org/10.1039/d1ra07719h.

[23] Meier A, Engeling K. Utilizing a CO2 carrier gas in a plasma assisted waste conversion test cell for space applications. Int. Conf. Environ. Syst., 2020. https://doi.org/https://hdl.handle.net/2346/86289.

[24] Rana T, Mallick AB, Kar S. Advancing carbon dioxide plasma gasification using graphite electrodes: a preheating study and in-situ carbon monoxide formation insights. Energy Convers Manag 2026;350:120972. https://doi.org/10.1016/j.enconman.2025.120972.

[25] Donaldson AL, Hagler MO, Kristiansen M, Jackson G, Hatfield L. Electrode erosion

phenomena in a high-energy pulsed discharge. IEEE Trans Plasma Sci 1984;12:28–38. https://doi.org/10.1109/TPS.1984.4316289.

[26] Ruj B, Ghosh S. Technological aspects for thermal plasma treatment of municipal solid waste—A review. Fuel Process Technol 2014;126:298–308. https://doi.org/10.1016/j.fuproc.2014.05.011.

[27] Sikarwar VS, Mašláni A, Hlína M, Fathi J, Mates T, Pohořelý M, et al. Thermal plasma assisted pyrolysis and gasification of RDF by utilizing sequestered CO2 as gasifying agent. J CO2 Util 2022;66:102275. https://doi.org/10.1016/j.jcou.2022.102275.

[28] Aikas M, Gimžauskaitė D, Tamošiūnas A, Uscila R, Snapkauskienė V. Thermal arc air plasma application for biomass (wood pellets) gasification. Clean Technol Environ Policy 2024;26:31–43. https://doi.org/10.1007/s10098-023-02566-4.

[29] Chen L, Yang L, Liu Z, Huang D, Qiu A. Erosion and Surface Morphology of the Graphite Electrodes in High-Current, High-Coulomb Transfer Gas Switch. IEEE Trans Plasma Sci 2018;46:3320–4. https://doi.org/10.1109/TPS.2018.2851307.

[30] Inagaki M, Kang F. Chapter 3 - Engineering and Applications of Carbon Materials. In: Inagaki M, Kang F, editors. Mater. Sci. Eng. Carbon Fundam. (Second Ed. Second Edi, Oxford: Butterworth-Heinemann; 2014, p. 219–525. https://doi.org/10.1016/B978-0-12-800858-4.00003-6.

[31] Tamošiūnas A, Milieška M, Gimžauskaitė D, Aikas M, Uscila R, Zakarauskas K, et al. Plasma Gasification of Medical Plastic Waste to Syngas in a Greenhouse Gas (CO2) Environment. Sustainability 2025;17. https://doi.org/10.3390/su17052040.

[32] Yousef S, Tamošiūnas A, Aikas M, Uscila R, Gimžauskaitė D, Zakarauskas K. Plasma steam gasification of surgical mask waste for hydrogen-rich syngas production. Int J Hydrogen Energy 2024;49:1375–86. https://doi.org/10.1016/j.ijhydene.2023.09.288.

[33] Pitrez P, Monteiro E, Rouboa A. Numerical analysis of plasma gasification of hazardous waste using Aspen Plus. Energy Reports 2023;9:418–26. https://doi.org/10.1016/j.egyr.2023.05.262.

[34] Okati A, Khani MR, Shokri B, Monteiro E, Rouboa A. On the operating parameters for hydrogen-rich syngas production in a plasma co-gasification process of municipal solid wastes and polypropylene using a constrained model in Aspen plus. J Energy Inst

2023;107:101173. https://doi.org/10.1016/j.joei.2023.101173.

[35] Mazzoni L, Janajreh I. Plasma gasification of municipal solid waste with variable content of plastic solid waste for enhanced energy recovery. Int J Hydrogen Energy 2017;42:19446–57. https://doi.org/10.1016/j.ijhydene.2017.06.069.

[36] Yadav A, Barath VR, Kar S, Kumar M. Cathode shape determines efficiency and arc-root attachment in thermal plasma torch – A numerical investigation. Thermochim Acta 2025;751:180082. https://doi.org/10.1016/j.tca.2025.180082.

[37] Yadav A, Karmakar S, Kar S, Kumar M. Numerical modelling of a direct current non-transferred thermal plasma torch for optimal performance. Contrib to Plasma Phys 2023;63:e202200088. https://doi.org/10.1002/ctpp.202200088.

[38] Roberta B, Barbalace C. EnvironmentalChemistry.com 2003:23–5.

[39] Qinglin Z, Liran D, Kentaro U, Yang W, Blasiak W. Process modelling and performance analysis of a PGM gasifier. 10th Conf. Energy a Clean Environ. Lisbon, Port., 2009.

[40] Kundu K, Kumar A, Kodamana H, Pant KK. Obtaining high H2-rich syngas yield and carbon conversion efficiency from biomass gasification: From characterization to process optimization using machine learning with experimental validation. Fuel 2024;378:132931. https://doi.org/https://doi.org/10.1016/j.fuel.2024.132931.

[41] Aguado R, Escámez A, Jurado F, Vera D. Experimental assessment of a pilot-scale gasification plant fueled with olive pomace pellets for combined power, heat and biochar production. Fuel 2023;344. https://doi.org/10.1016/j.fuel.2023.128127.

[42] Tamošiūnas A, Gimžauskaitė D, Aikas M, Uscila R, Snapkauskienė V, Zakarauskas K, et al. Biomass gasification to syngas in thermal water vapor arc discharge plasma. Biomass Convers Biorefinery 2023;13:16373–84. https://doi.org/10.1007/s13399-023-03828-3.

[43] Ponduri S, Becker MM, Welzel S, van de Sanden MCM, Loffhagen D, Engeln R. Fluid modelling of CO2 dissociation in a dielectric barrier discharge. J Appl Phys 2016;119:93301. https://doi.org/10.1063/1.4941530.

[44] Kozák T, Bogaerts A. Splitting of CO2 by vibrational excitation in non-equilibrium plasmas: a reaction kinetics model. Plasma Sources Sci Technol 2014;23:45004. https://doi.org/10.1088/0963-0252/23/4/045004.

[45] Rath S, Kar S. Generation of sound waves in a continuous-wave mode microwave atmospheric pressure plasma jet. Phys Fluids 2025;37:117113. https://doi.org/10.1063/5.0293788.

[46] Zhou T, Yang Q, Yuan T, He H, Liu H. Plasma characteristics of medium voltage AC air arc discharge and its application on arc electrical parameters calculation. J Phys D Appl Phys 2023;57:25202. https://doi.org/10.1088/1361-6463/ad00c8.

[47] Hofmann S, van Gessel AFH, Verreycken T, Bruggeman P. Power dissipation, gas temperatures and electron densities of cold atmospheric pressure helium and argon RF plasma jets. Plasma Sources Sci Technol 2011;20:65010. https://doi.org/10.1088/0963-0252/20/6/065010.

[48] Central Pollution Control Board. “Selection Criteria for Waste Processing Technologies.” 2020.

[49] Bureau of Indian Standards. Indian Standard - Methods of Test for Coal and Coke. 1984.

[50] Bureau of Indian Standards. Indian Standard METHODS OF TEST FOR COAL AND COKE PART IV ULTIMATE ANALYSIS(First Revision). 1974.

[51] Bureau of Indian Standards. Indian standard, Methods of test for Coal & coke. vol. IS:1350. 1999.

[52] Bureau of Indian Standards. Method of Test for Coal and Coke Part Iii Determination of Sulphur. 1969.

[53] Bureau of Indian Standards. Methods of Test for Coal and Coke, Part II: Determination of Calorific Value. 1975.

[54] Komuro A. Recent advances in surface charge dynamics in dielectric barrier discharge: future strategies for control and technological optimisation. J Phys D Appl Phys 2025;58:133003. https://doi.org/10.1088/1361-6463/adb29e.

[55] Ma S, Cheng H, Li J, Xu M, Liu D, Ostrikov K. Large-scale ion generation for precipitation of atmospheric aerosols. Atmos Chem Phys Discuss 2020;2020:1–22. https://doi.org/10.5194/acp-20-11717-2020.

[56] Park HS, Kim CG, Kim SJ. Characteristics of PE gasification by steam plasma. J Ind Eng Chem 2006;12:216–23.

[57] Cao C, Bian C, Wang G, Bai B, Xie Y, Jin H. Co-gasification of plastic wastes and soda lignin in supercritical water. Chem Eng J 2020;388:124277. https://doi.org/10.1016/j.cej.2020.124277.

[58] Collard F-X, Blin J. A review on pyrolysis of biomass constituents: Mechanisms and composition of the products obtained from the conversion of cellulose, hemicelluloses and lignin. Renew Sustain Energy Rev 2014;38:594–608. https://doi.org/10.1016/j.rser.2014.06.013.

[59] Mallick R, Vairakannu P. Experimental investigation of acrylonitrile butadiene styrene plastics plasma gasification. J Environ Manage 2023;345:118655. https://doi.org/10.1016/j.jenvman.2023.118655.

[60] Saleem F, Zhang K, Harvey AP. Decomposition of benzene as a tar analogue in CO2 and H2 carrier gases, using a non-thermal plasma. Chem Eng J 2019;360:714–20. https://doi.org/10.1016/j.cej.2018.11.195.

[61] Mallick R, Vairakannu P. CO2 plasma gasification of bakelite-based electrical switch waste feedstock. J Clean Prod 2023;423:138813. https://doi.org/10.1016/j.jclepro.2023.138813.

[62] Kang S, Byun J, Kim M, Lee S. Sustainable chemical processing of municipal plastic waste: Techno-economic and life cycle assessment of incineration, gasification, and pyrolysis oil production. Int J Hydrogen Energy 2025;137:652–64. https://doi.org/10.1016/j.ijhydene.2025.05.022.

[63] Buttler A, Spliethoff H. Current status of water electrolysis for energy storage, grid balancing and sector coupling via power-to-gas and power-to-liquids: A review. Renew Sustain Energy Rev 2018;82:2440–54. https://doi.org/10.1016/j.rser.2017.09.003.